



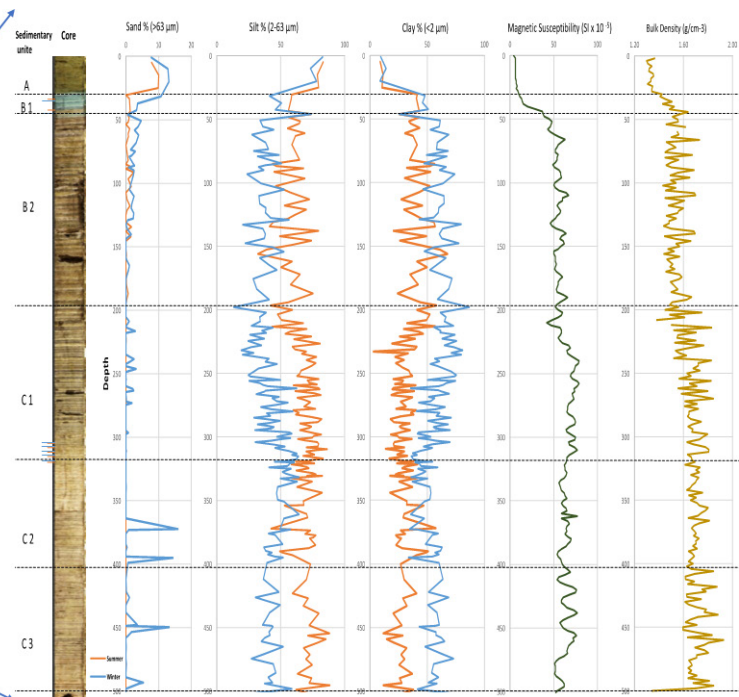
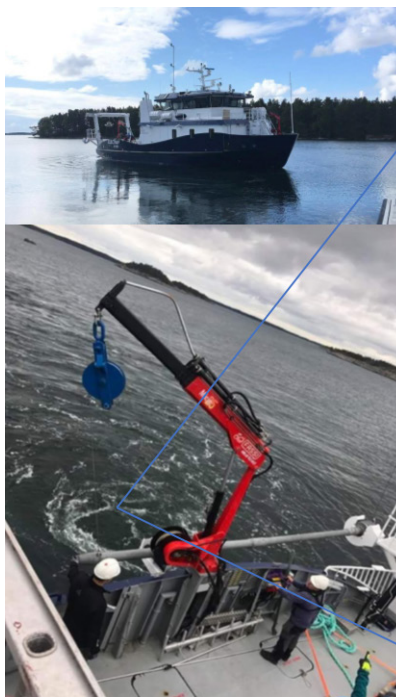
Stockholm
University

Master Thesis

Degree Project
in Marine Geology 30 hp

Younger Dryas-Early Holocene environmental conditions in a 299 year varve-record from Asköfjärden, Southern Stockholm Archipelago

Fatemeh Ghasemi



Stockholm 2018

Department of Geological Sciences
Stockholm University
SE-106 91 Stockholm
Sweden

Abstract

Large parts of the Baltic Sea basin are covered by glacial clay. Varved sediments have been studied for decades both in terrestrial sections and marine cores but data on marine glacial clay and varve stratigraphy is limited. Glacial clay varves is also useful as a climate proxy, as the difference in varve thickness can be plotted against time to determine climate variability.

The present study has examined 299 glacial varves from a sediment core from Asköfjärden, southern Stockholm archipelago. Grain size variations in these glacial varves throughout the core and total C & N content in a few samples were measured. The core indicated three distinct lithological units, where the lowermost unit (C) was divided into three subunits, and the middle unit (B) was divided into two subunits. There is a sharp contact with a thin sand layer between the glacial varves in unit B1 and a greyish layer in lowermost unit A, which indicates erosion and a likely hiatus between unit A and B.

A varve thickness diagram was created and compared with previous published clay varve diagrams from the region, to estimate the time of varve formation. The varve chronology spans a period from ca 11488 to 11787 cal yr BP. The formation of the oldest part of the core is characterized by a varve thickness ≤ 1 cm and occurred during the end of the Baltic Ice Lake (BIL) and includes the last BIL drainage at the end of the Younger Dryas cold period. The youngest varves in the core formed during the early Holocene warming period by a varve thickness between 3-5 cm. Post-drainage glacial varves show higher carbon and nitrogen values compared to pre-drainage sediments. Generally winter layers have finer sediment compared to summer layer during the whole core independent to warmer or colder climate but in handful of places show a reverse trend which could be affected by some intra seasonal storm events or that some winters became warmer. Winter layers demonstrate higher carbon and nitrogen values compared to summer layers because diatoms and phytoplankton bloom in the spring/summer and get deposited in the autumn/winter.

Paleoclimatic interpretation of the new varve chronology indicates that the nearest glacier front receded rapidly when ice receded on the northern Mt Billingen after final BIL drainage. In this core, the BIL drainage was recorded in varve number 107 which coincide with 11594 cal yr BP.

Since the core located in an area which is higher than surrounding area, an ongoing erosion of the seafloor display on the top of this core in unit A. The whole core except unit A consists mostly of clay and very fine silt particles which formed a low permeability condition and as a result, no evidence of groundwater seepage could be found at the core location place.

Contents

Abstract.....	1
1. Introduction.....	4
1.1. Background.....	6
1.2. Baltic sea history.....	7
1.2.1. Baltic ice lake.....	7
1.2.2. Yoldia sea.....	8
1.2.3. Ancylus lake.....	9
1.2.4. Littorina sea.....	10
2. Materials and methods	11
2.1. Coring	11
2.2. Acoustic mapping method	11
2.3. Geophysical measurements	15
2.3.1. Bulk density (Gamma density)	15
2.3.2. Magnetic susceptibility	15
2.4. Core description	15
2.4.1. Unit A.....	17
2.4.2. Unit B.....	17
2.4.2.1. Subunit B1	17
2.4.2.2. Subunit B2	17
2.4.3. Unit C.....	17
2.4.3.1. Subunit C1	17
2.4.3.2. Subunit C2	18
2.4.3.3. Subunit C3	18
2.5. Varve thickness measurement	20
2.6. Core sub-sampling	20
2.7. Grain size measurement.....	20
2.7.1. Measurement procedure.....	22
2.7.2. Data export.....	23
2.8. Carbon and nitrogen methods	24
3. Result.....	24
3.1. Stratigraphy	24
3.2. Varve thickness measurement	25
3.3. Grain size, magnetic susceptibility and bulk density	27
3.4. Organic carbon and nitrogen	33
4. Discussion	34
4.1. Stratigraphy	34
4.2. Varve thickness measurement	35
4.3. Grain size, magnetic susceptibility and bulk density	37
4.4. Organic carbon and nitrogen	40
5. Conclusion	41
Acknowledgements	43

References	43
Appendix.....	47
Appendix 1.....	47
Appendix 2	52
Appendix 3.....	52

1. Introduction

In the past century, our understanding of the Baltic Sea's development during the last deglaciation has increased at a remarkable rate. A large body of research has studied changes in sea level, salinity and grain size variation driven by global climate and glacial isostasy after the Baltic Sea appeared underneath the Weichselian Ice Sheet between ca. 15000 - 11600 cal years BP (Björck, 1995; Björck et al., 1996; Andrén et al., 1999, 2002).

There has been a wide interest of varved clay chronology in northern European countries for dating of the Weichselian deglaciation and its shoreline displacement. Glacial varves are valuable archives of the past climate and has therefore become a central focus in paleolimnological research. Annually laminated sediments represent for example when a drainage event occurred, how fast glaciers recede, past productivity or erosional input, and gives a continuous timescale and information about the types of minerals and fossils. These glacial sediments can also be significant sources of groundwater.

Glacial varves were used as a climate proxy for the first time by Swedish geologist De Geer in 1884. He obtained a chronology by measuring the thickness of the varves in different localities and created the Swedish Time Scale, the world's first absolute geochronology. A varve is composed of an annual sediment layer. Summer layers include more sandy or silty particles (lighter color) and winter layers contain finer sediment like clay particles (darker color). Differences in glacial varve minerals can also give different colors depending on their origin, for example a brownish color change to grey after the final drainage of the Baltic Ice Lake (BIL) (Strömberg 1992; Brunnberg 1995; Andrén et al., 1999). The difference in varve thickness can be plotted against time to determine climate variability (Andrén et al. 1999, 2002). A long climate pattern can be assembled by using the changes in varve thicknesses (De Geer, 1884). But it is impossible to find a complete record at one place due to ice advances and retreat and because the ice recession eventually makes the location too distal to form varves. Therefore, sediment cores were taken in different localities and correlated to each other in order to construct as long records as possible. The present Swedish varve chronology consists of more than 1000 varve-thickness diagrams at different localities from the southernmost part of Sweden to northern Sweden (Andrén et al., 2002).

Groundwater is an important resource in these glacial deposits. Understanding how these sediments were deposited, previous relative sea level history, shoreline and what their geometry is in subsurface is important to study this resource (Jakobsson et al., 2016). When shallow glacial melts, it forms glacial till which includes all grain size particles. These primary sediments are later out washed by running water and has formed a sorted layer. The size and shape of the sediment particles affect the porosity. When particles have almost the same size and shape, there is larger open spaces in between since the particles do not fit together well. The more porous the sediment, the more water it can hold, and transport. The rate of water infiltration into the ground is called permeability (Tavenas et al., 1984). Clay and sand are both very porous materials but clay have a low permeability compared to sand (Beard and Weyl, 1973). Therefore, sand makes an excellent groundwater reservoir because of its good permeability. Clay deposits have high porosity, but because they have little permeability, they do not form groundwater table, despite

the large volume of water they may contain, and are considered as impervious to the material (Beard and Weyl, 1973; Piotrowski, 1997). This thesis gives some basic characteristics and chronological framework for further studies of ground water features.

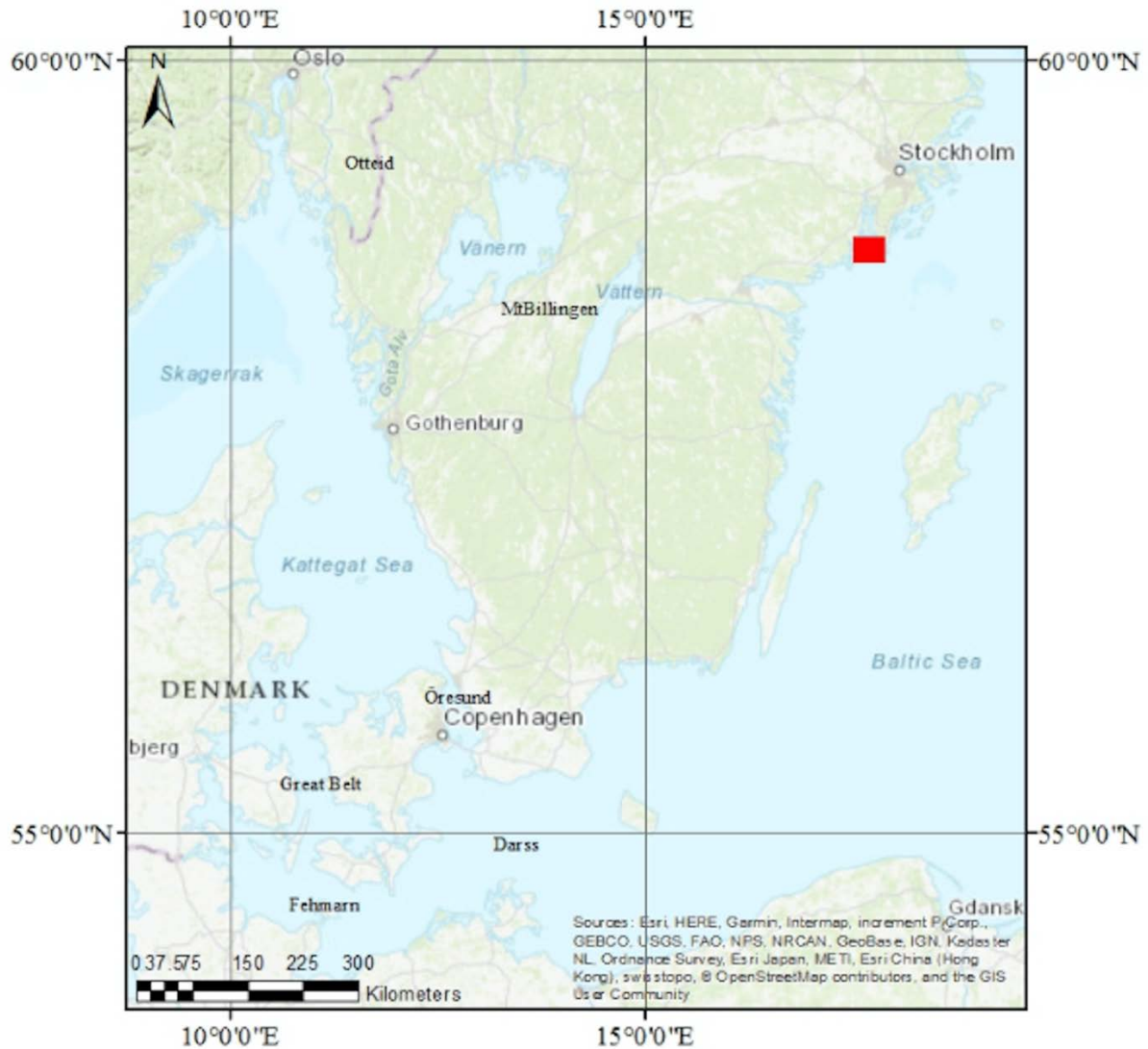


Figure 1. A topography map over the Baltic Sea region include the geographic names and locations that were key sites during the stages of the Baltic Sea. Location of study area (red box: map over Askö in the archipelago outside of Trosa, see where Askö is located in relation to Stockholm).

During the last decade, there has been a large interest in terraces on the seafloor around Askö which are interpreted to be formed by flowing groundwater. Geophysical investigations to examine this have been done recently using modern high- resolution systems, as multi-beam echo sounders and sub-bottom profilers (Jakobsson et al., 2016).

In 2017, were 2 sediment cores obtained to investigate possible groundwater seepage sites and sediment stratigraphy in the Askö region (Figure 1). The first one was extracted on a terrace and the second one was obtained in an area located higher than the surrounding seafloor and as a

consequence could be more exposed to erosion. The second core, a 5 meters long sediment core was investigated in this study. This core (Asko2017HT-02-GC-1) was composed mainly of varved glacial clays. This thesis describes sedimentological and stratigraphic investigations of a sequence of 299 glacial varves from a five-meter gravity core in a terrace area near Askö archipelago outside of Trosa, southern Stockholm (Figure1). The objectives of this project are:

- to measure grain size variations and determine total carbon and nitrogen content within and between selected glacial varves,
- to produce a glacial varve chronology and correlate it with the existing varve chronology,
- to interpret the varve deposition in terms environmental changes such as glacial melt rate and relative distance to the ice margin,
- to identify possible permeable layers that could have permitted ground-water flow.

1.1. Background

The Baltic sea has several sub-basins (Figure 2): The Danish Straits, the Baltic Proper, the Gulf of Riga, the Archipelago Sea, the Gulf of Finland and the Gulf of Bothnia (divided into the Bothnia Sea and the Bothnia Bay) (Weckström et al., 2017). The Baltic Sea drainage area is almost 412,560 km² (Seifert and Kayser, 1995).

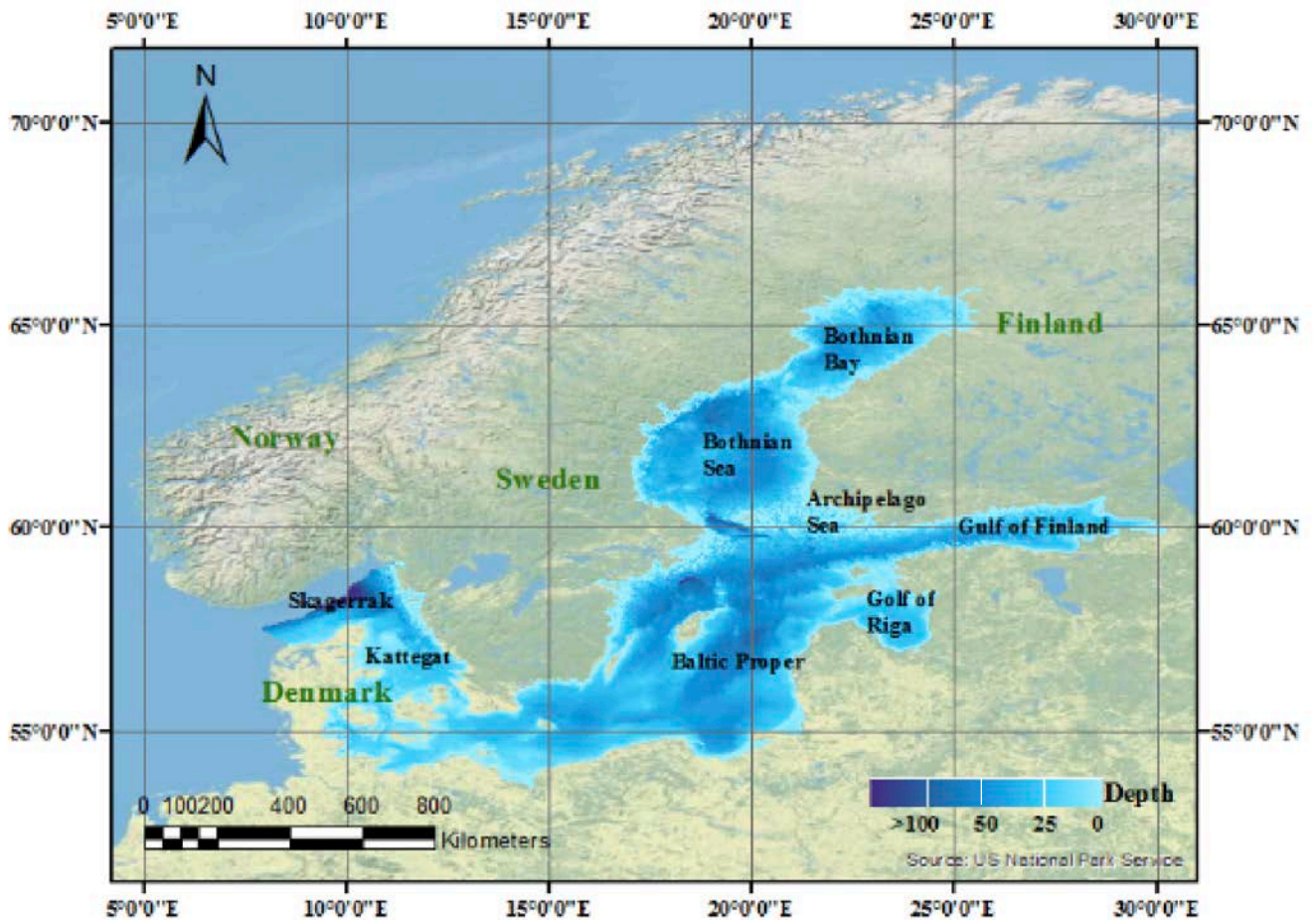
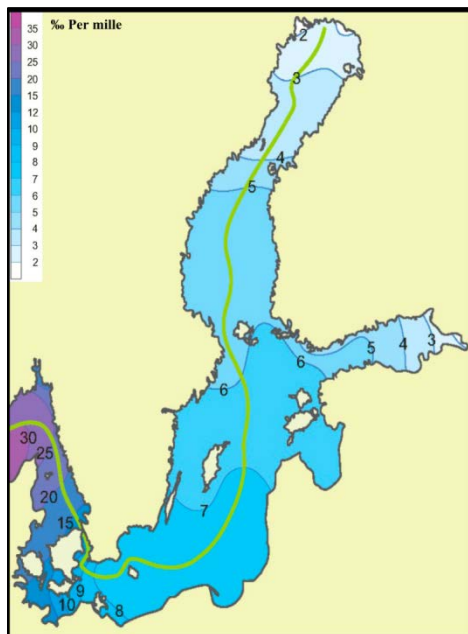


Figure 2. A topography map over the Baltic Sea region include the sub-basins.



The salinity in the Baltic sea is around 15-20 ‰ in the Danish Straits (Figure 3) and decreases to 1- 4 ‰ in the Gulf of Bothnia because of freshwater input from rivers (Voipio, 1981). Salinity varies with location, depth and time, a variation caused by different factors such as meltwater amount, isostasy and eustasy changes (Gustafsson and Westman, 2002; Björck, 1995), the volume of water inflows and outflows from and to the North Atlantic (Westman and Sohlenius 1999), and variations in depths and widths of the thresholds between the sea and the Baltic basin (Andrén et al., 2011).

Figure 3. The surface salinity of the Baltic Sea decreases from Öresund to Bothnian; (modified from Winsor et al., 2001, Fonselius, 1996).

1.2. Baltic sea history

Scandinavia had been covered by a heavy inland ice (Saarnisto and Saarinen, 2001) before the beginning of a stepwise ice recession on the Baltic basin at 15000 cal yr BP (Winterhalter et al., 1992; Björck, 1995). The ice retreat began first at Skåne and continued to South-central of Sweden and finally reached Ångermanland (Andrén et al. 1999, 2002; Björck, 1995). Internal deformation, basal sliding and bed deformation destroyed almost all traces older than 15000-14000 cal yr BP years old during the last deglaciation cycle (Björck, 1995).

1.2.1. Baltic ice lake (BIL)

The proglacial Baltic Ice Lake appeared after regression of the southwestern part of the Scandinavian Ice Sheet at ca 17000 cal yr BP, and existed about 15000-11600 cal yr BP (Björck, 1995; Björck et al., 1996, Andrén et al. 1999). The Kattegatt-Skagerrak formed the primary connection between the Baltic basin and the Atlantic when the pressure of the ice disappeared in Öresund area between 17000-16000 cal yr BP (Figure 4). Öresund began to uplift and formed the first land between Malmö and Copenhagen (Björck, 1995; Lundqvist and Wohlfarth, 2001; Houmark-Nielsen and Kjær, 2003). This continuing uplift made the Öresund threshold gradually shallower and the water level increased inside the threshold at 14000 cal yr BP (Björck, 1995). When ice receded in north of the Danish Straits and the Öresund threshold created was a lake called the Baltic Ice Lake (Björck et al., 1996). The Baltic lake level was 100 meters above the sea level in the west (Lambeck and Chappell, 2001). The sediment accumulation rate was very high due to the rapidly melting Scandinavian ice sheet, and the sediments were inorganic (Berglund et al. 2005; Andrén et al. 2007b, Björck, 1995, Muschitiello et al., 2015).

The Billingen mountain between the two large lakes Vättern and Vänern became a dam between the Skagerrak and the BIL. When the ice margin retreated to reach the northern Mt Billingen, a new outlet for the Baltic Sea in addition to the Öresund threshold was opened around 13000 cal yr BP (first drainage of the BIL). This ocean outflow decreased water level about 10 meters (Adriellsson 1984; Björck, 1995).

During the Younger Dryas cold period, and ice advance closed the Billingen sill (Björck et al., 1996, Houmark-Nielsen et al., 2003), the BIL water level rose above the sea level outside, and as a consequence, water outflowed over the Öresund threshold again at c. 12800 cal yr BP (Björck, 1995). Water outflow continued through the Öresund threshold because of isostatic effects gradually increasing the water level of the southern BIL. Final drainage occurred at the end of the Younger Dryas (Figure 4) (Björck, 1995). The ice would recede rapidly until opened a threshold at Mt. Billingen and water outflow to Atlantic through this channel about 11700 cal yr BP (Björck et al. 1996; Andrén et al. 2011). Water drained over 7000 km³ (Strömberg 1992; Jakobsson et al. 2007) dropped by 25 meters during the 1-2 years (Svensson 1991). The Yoldia Sea stage begin after this drainage.

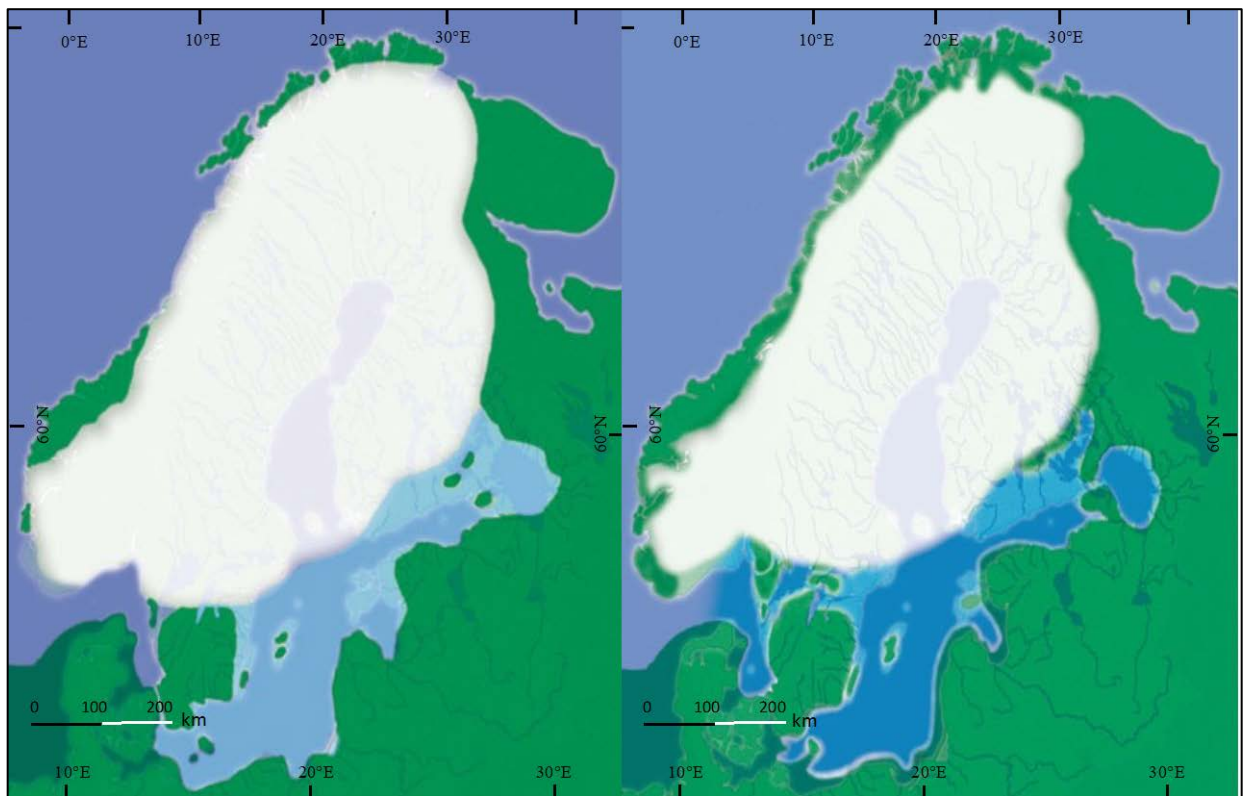


Figure 4. Paleogeographic reconstructions of the Baltic Ice Lake at ca 11700 cal yr BP, before the final (25 m) drainage (left), The Baltic Yoldia stage at ca 11100 cal yr BP during its brackish phase (right); (modified from Andrén, 2003a).

1.2.2. Yoldia sea

The early Holocene climate warming in Scandinavia was triggered by ocean surface warming and a rapid ice regression at c. 11600 cal yr BP (Björck, 1995). The Yoldia Sea stage began at this point and lasted about 900 years (Figure 4). When the ice receded at the north side of the

Skagerrak, it opened a pathway between the Baltic basin and Skagerrak (Björck,1995; Andrén et al., 2011). The straits between lake Vänern and the Baltic opened up slowly and marine inflow increased gradually in the Baltic basin for ca 250 years (the Yoldia Sea fresh water phase). The climate got colder again due to the Preboreal Oscillation when less melt water and ice advance altered the Baltic basin water fresh phase to a brackish phase (Björck et al. 1996, 1997). This alteration created a nutritious environment (the Yoldia Sea Brackish water phase for approximately 150 years) (Andrén et al., 1999; Björck,1995). The amounts of fossils increased due to nutrient-rich water inflow from Atlantic (Schoning and Wastegård 1999). Mussels (*Portlandia*), foraminifera and diatoms emerged in this brackish condition. Yoldia's name came from the shell named *Portlandia* (*Yoldia*) *arctica*. The land uplift continued in south-central of Sweden and the straits between lake Vänern and the Skagerrak became shallower. Since the straits closed on the west of Lake Vänern, marine water couldn't inflow in to the Baltic anymore (a new Yoldia Sea fresh water phase). During this time, the global sea level raised 2 cm per year due to the melting of Northern Hemisphere ice sheets, but the land uplift was faster than sea level rise (Andrén et al. 1999, 2002; Björck,1995). This stage ended with outflowing water from the Baltic by water level increasing at 10700 cal yr BP. The last brackish phase was a short period due to the rapid land uplift and the Baltic now entered to the Ancyclus lake stage (Andrén et al., 2011; Björck,1995).

1.2.3. Ancyclus lake

The turning point to this Baltic stage started with isostatic rebound on the sills/straits. The uplift rate in SW Sweden was faster than the global sea level rise, the outlets west and southwest of Lake Vänern became shallower and narrower until a new damming formed by isostatic effects (Figure 5). The water level rose rapidly at 10300 cal yr BP (Andrén et al. 2007; Björck,1995). Differential isostatic uplift caused a tilting of Scandinavia, which led to transgression in the south and regression on the north (Figure 5). The Ancyclus lake stage began with this tilting effect at 10700 cal yr BP and lasted for almost 1000 years (Björck,1995; Andrén et al., 2000; Berglund et al., 2005). During the Yoldia Sea fresh water phase and the Ancyclus Lake decreased organic carbon deposition. Differential uplift ratio was the most important factor for the Ancyclus transgression difference between regions and was strongest in the south (Björck,1995). Sediment deposits record an oligotrophic environment with limpet fossils named *Ancyclus* during this stage (Voss et al. 2001; Andrén et al. 2000; Björck,1995). The Ancyclus lake level was higher than the sea level in the Skagerrak and water outflowed through three straits at Otteid, Göta Älv and Uddevalla (Björck,1995). The transgression phase ended when the Ancyclus lake water level was 10 m above the sea level outside at c. 10200 cal yr BP (Björck et al. 2008; Björck,1995). Land uplift and the Ancyclus drainage formed a north-south land bridge between Lake Vänern and the Ancyclus Lake (Andrén et al. 2007; Björck,1995; Andrén et al. 2011).

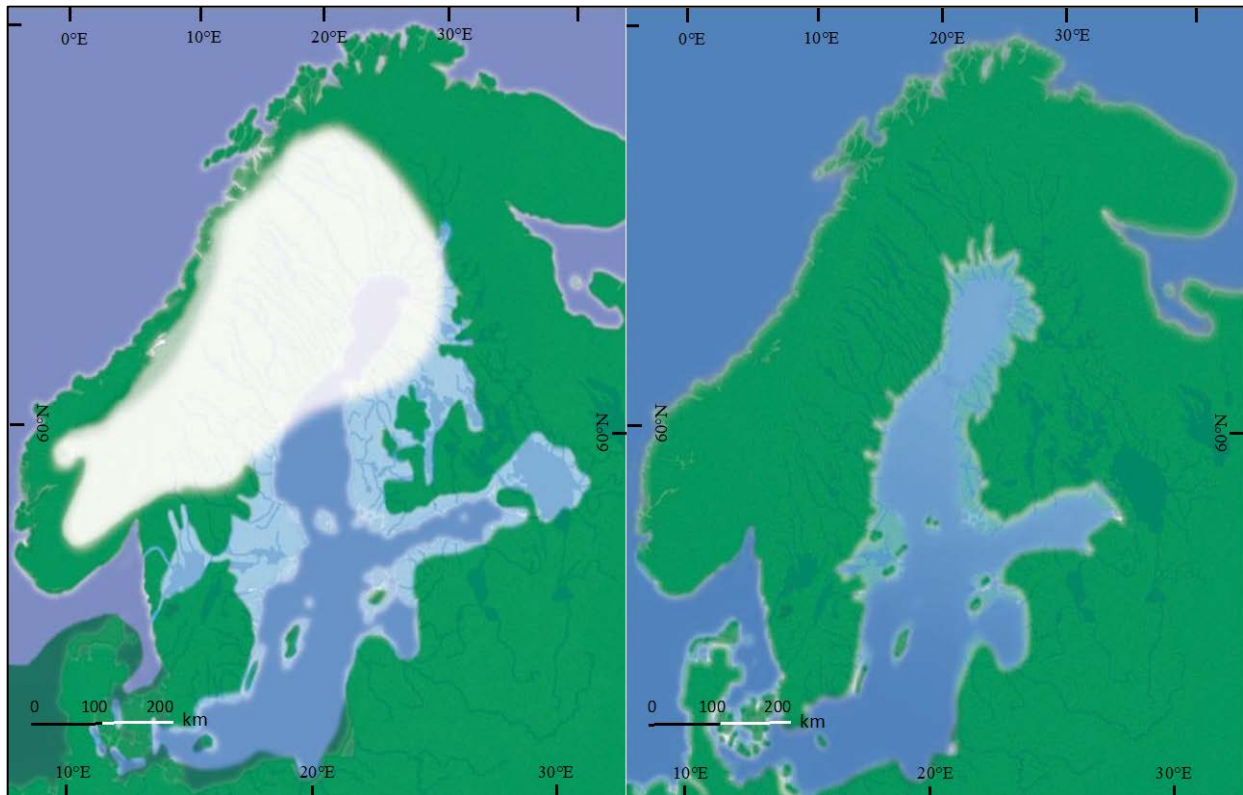


Figure 5. The Ancylus stage at 10500 cal yr BP during the transgression (left), Littorina Sea during most saline phase at ca 6500 cal yr BP (right); (modified after Andrén, 2003a).

1.2.4. Littorina sea

The Littorina sea formed approximately at 9800 cal yr BP (Andrén et al., 2000; Berglund et al., 2005). The Littorina Sea stage can be classified into three parts; Initial Littorina Sea (fresh-brackish, 9800-8500 cal yr BP), the Littorina Sea (brackish-marine, 8500-7500 cal yr BP) and the Post Littorina Sea (brackish, 7500-6000 cal yr BP) (Andrén et al. 2000a; Berglund et al. 2005). This stage began with a gradual transition from the oligotrophic Ancylus Lake to a brackish Littorina Sea in almost 1500 years which emerged by a gradual increase of organic content in sediments (Björck 2008; Björck 1995; Andrén et al. 2011).

It became rapidly warmer during a short time at the beginning of this stage (brackish-marine), which known as Littorina transgressions between 8500-7500 cal yr BP (Björck,1995; Berglund et al. 2005). This warming caused a lot of ice melting on the Laurentide and Antarctic ice sheet, and sea level rose faster than land uplift. Therefore, marine water flowed in through Öresund and the Great Belt Straits (brackish-marine) which caused a 10-meter transgression in these straits and an increase in water depth (Björck,1995; Berglund et al. 2005).

The Post Litorina sea stage had the highest salinity in the whole Baltic history (brackish) at almost 7500-6000 cal yr BP (Figure 5) (Björck,1995; e.g., Westman and Sohlenius 1999). High salinity and mid-Holocene warmer climate formed an organic-rich environment (Sohlenius and Westman 1998, Zillén et al. 2008). The high productivity of organic material and strong stratification caused anoxic conditions. Lesser mixing in the water column resulted in higher productivity in deeper parts (denser water sank down due to higher density) (Bianchi et al. 2000,

Borgendahl and Westman 2006, Kunzendorf et al. 2001). The organic productivity in saltwater increased, which consumed all oxygen during its break-down, and formed anoxic conditions on the sea bottom (>100 m) (Björck,1995). As a result, H₂S was reduced to FeS and formed laminated sediments (Bianchi et al. 2000, Borgendahl and Westman 2006, Kunzendorf et al. 2001). These laminated sediments are indicated by dark ferrous sulfide layers (Sohlenius et al. 1996). Sulfide banding can be distinguished from glacial varves because glacial varves change gradually between light to dark layer (summer and winter layers) compared to the sulfate boundary which display a sharp limit between dark and light layers; and sulfide boundaries has much more black borders than glacial varves (Björck,1995; Gustafsson and Westman 2002; Sohlenius et al., 2001).

2. Material and methods

2.1. Coring

The core Asko2017HT-02-GC-1 was obtained by gravity coring in September 2017 during the Marine Geophysical Mapping Methods course in Asköfjärden at a water depth of 17 meters in the southern Stockholm archipelago outside of Trosa in Askö. After retrieving, the core was divided lengthwise into 4 sections, where the uppermost section was only 0.59 meters (Figure 10). These sections were stored at 4° C in the shipboard refrigerator, and later in cold storage at the Department of Geological Sciences, Stockholm University. The sediment coring characteristics are presented in Table 1.

Station names	Asko2017HT-02-GC-1
Type of coring	Gravity Core
Latitude	058°51.087' E
Longitude	017°41.164' N
Core head weight	473 kg
Water depth	17 m
Liner type	PVC
Core catcher type	Finger
Core bottom date	06/09/2017
Total core length	5.09 meters

Table 1. Sediment core characteristics Asko2017HT-02-GC-1.

2.2. Acoustic mapping methods

During the fieldwork in Askö 2017 about 1.5 km² was mapped with multibeam sonar within two days (Figure 6). The cruise was done by R/V Electra to survey the seafloor shape and the marine stratigraphy by using multi beam echo sounder (MBES), Kongsberg EM 2040 multibeam with a frequency between 200-400 kHz and 0.4°*7° beam width, and sub-bottom profiles were obtained using a Kongsberg Topas PS40 with primary frequencies between 35-45 kHz, resulting in a secondary chirp signal between 2-10 kHz with 6 millisecond length. 2 gravity cores were extracted from locations identified in the acoustic data where possible groundwater outflow occurred. The first core (Askö2017HT-1-GC-1) was obtained on a terrace region and the second core (Askö2017HT-2-GC-1) was taken in an area that lies higher than the surrounding seafloor

since this area shows a clear stratigraphy in the Sub-bottom profile (Figure 7a). This study is focused on the second core which situated in northeast of Askö and northwest of Fifång island.

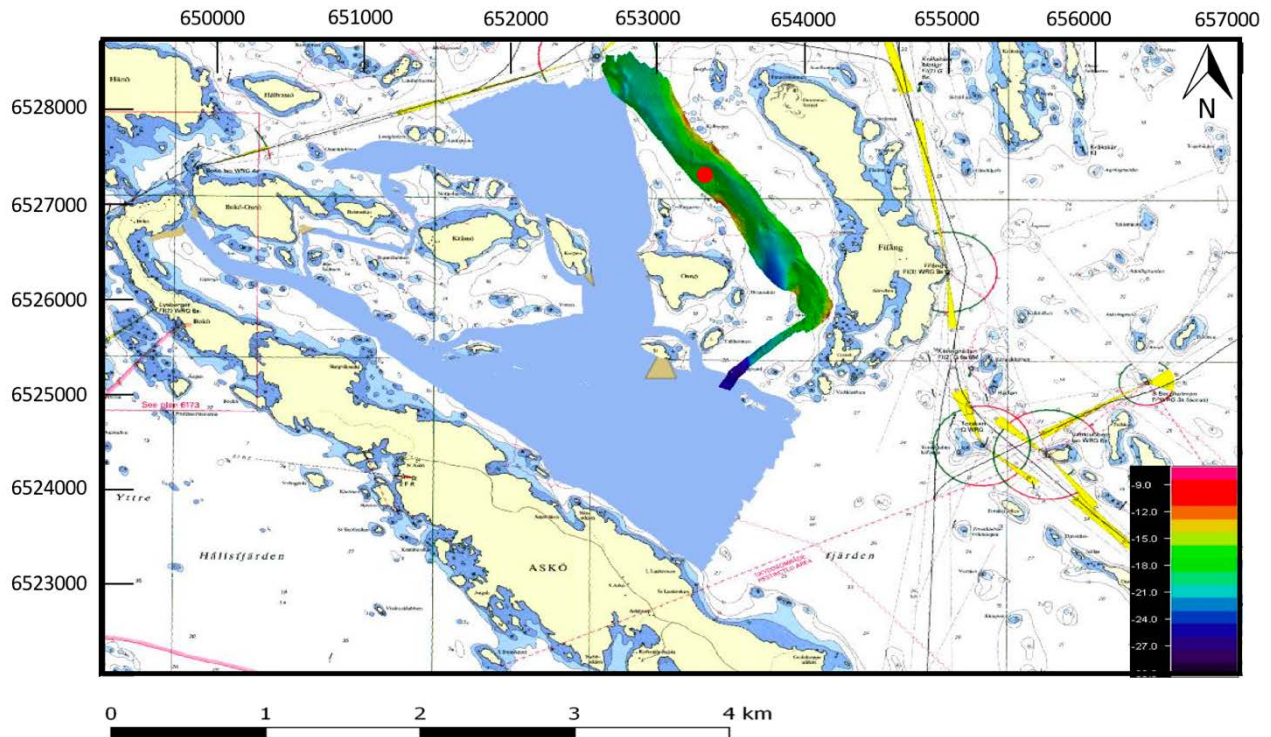


Figure 6. Topography map showing surveyed area; the rainbow color shows multibeam echo sounder data in Qimera which classify by depth (hot colors are shallower) and the red dot display core location. The blue surrounded area illustrates the previous MBES region.

The Core sample location is presented in the corresponding sub-bottom profile with the illustration of the estimated penetration of the core (Figure 7a). Based on the sub-bottom profiles, three different geophysical units were defined around the core location. Figure 5b represents a general result of collected sub-bottom data. Each lithological unit is separated by a distinct reflector. The first reflector represents the sea-bottom with a high impedance ratio. Unit 1 underlie this reflector and is interpreted to be postglacial clay. Unit two represents stratified sediments with high contrast in impedance values which is interpreted to be glacial clay, and the third unit is basement (bedrock). The highest contrast in impedance value shows in unit 2, which is interpreted as layered glacial clay and this unit is thicker than unit 1 and 3.

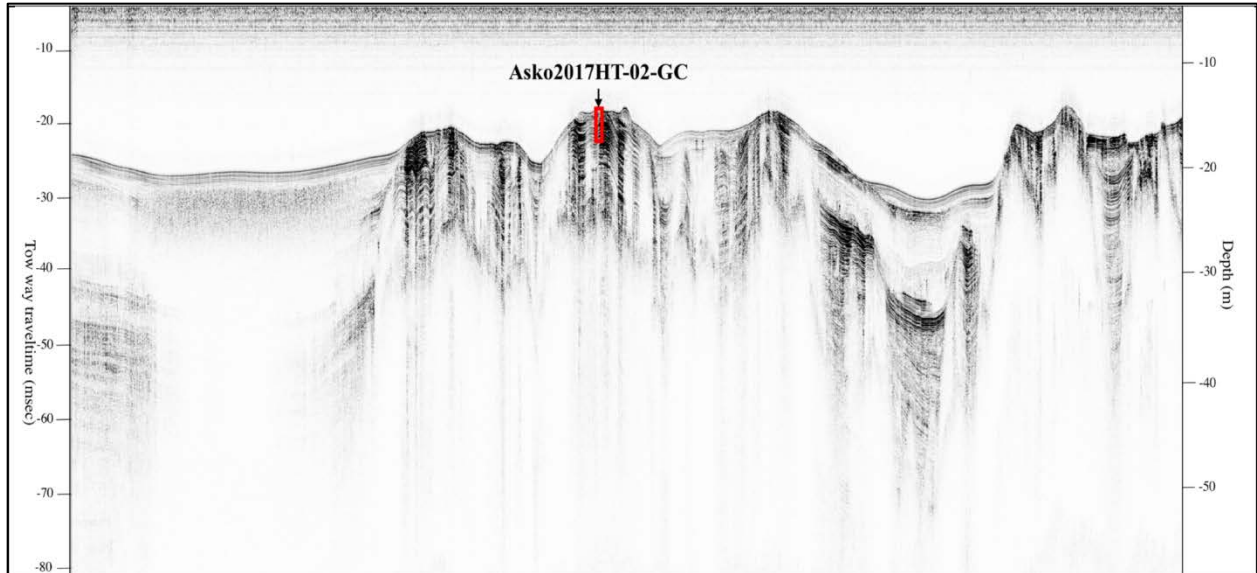


Figure 7a. Sub-bottom profile of the study area with the core location. The y-axis on the left shows seismic two-way travel time in milliseconds and the y-axis on the right shows depth in meters. Sub-seafloor acoustic map with characterize reflectors and units. Askö2017HT-2-GC-1 core location with estimated penetration shows with red box and black arrow.

The seafloor around Askö has been surveyed with single-beam echo sounder and side-scan sonar equipment in the beginning of the 1990s by Söderberg & Flodén (1991, 1995). They identified terraces and semi-circular depressions for the first time by interpreted maps of seabed geology. Most recently, marine geological surveys in Asköfjärden have been done by using modern high-resolution techniques such as multi-beam echo sounders and sub-bottom profilers by Jakobsson et al. (2016). The new technique provides a better resolution and more detailed acoustic seabed maps and as a result a better visualization. According to their analysis the terraces were semi-circular depressions about 1 m high and 10-100 m length. Jakobsson et al. (2016) identified variable vertical and horizontal blanked areas in the acoustic profiles (in glacial clay) which was interpreted as fluid discharge and seepage at the seafloor. These investigations have also revealed that terraces could be formed by flowing groundwater through silty permeable layers in glacial clay. Terraces were formed above sediments with fluid escape, and these sediments erosion were deformed beneath layers. As a result, overlying layers were collapsed which has formed depression on the seafloor. The current sub-bottom profile shows similar deformation layers and fluid signatures as Jakobsson et al. (2016) found. Figure 7b shows the similar features as deformed layers and blanked areas which interpreted to be formed by groundwater flow in glacial clay.

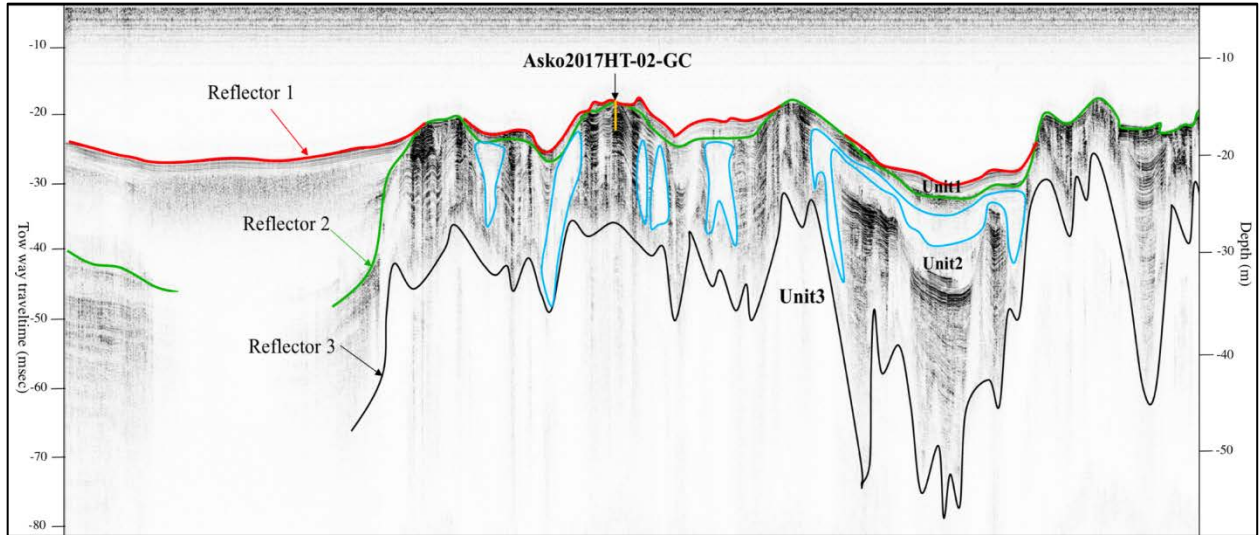


Figure 7b. Sub-seafloor acoustic map with characterize reflectors and units. Askö2017HT-2-GC-1 core location with estimated penetration shows with orange line and black arrow. The blue surrounded area illustrates the possible fluid flow.

The MBES bathymetry produces three-dimensional high-resolution digital bathymetry models of the seafloor but it requires post-processing before interpretation. Raw MBES data was processed on the Qimera software version 1.5.3. for removing any prominent outlier values. For cleaning multibeam surface on Qimera was SWEREF99 projection used with a meridian of 18° E. Rainbow colors on figure 5 represent the survey area in Qimera, classified by depth (hot colors are shallower). The Fledermaus software version 7.6.3 was used afterward for analysis of the core sites along the swath (Figure 8).

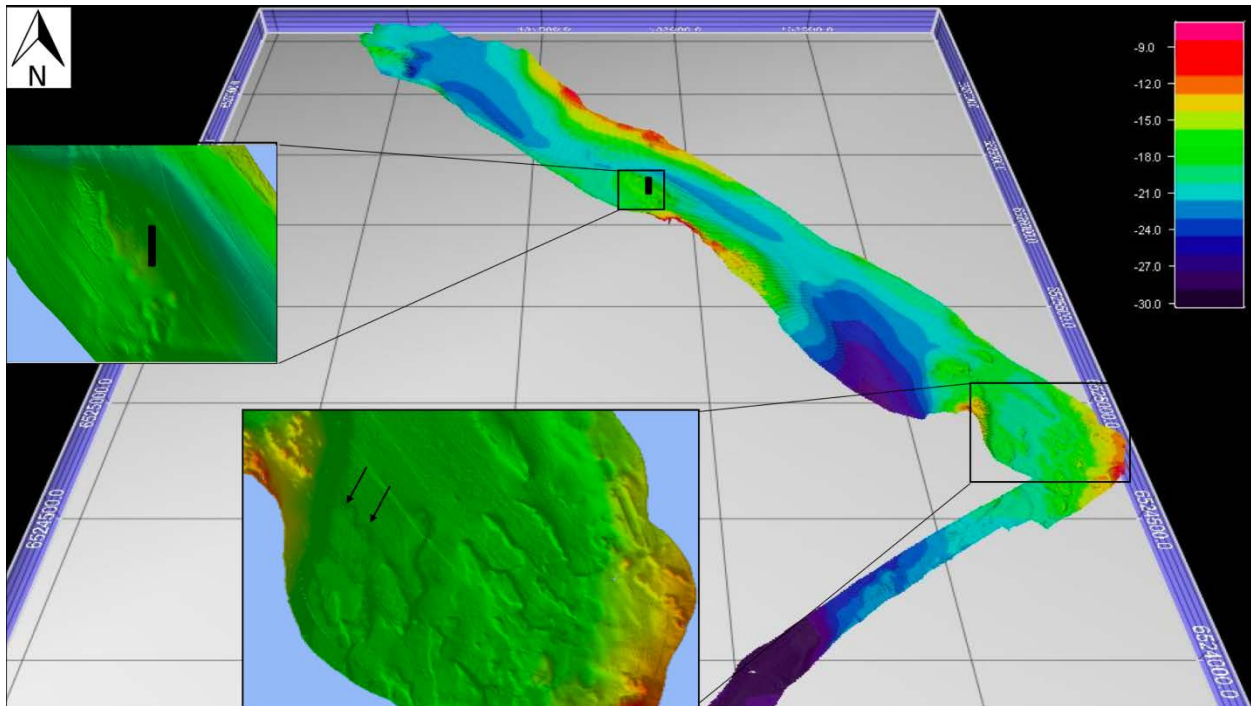


Figure 8. Map over the surveyed area done by Fledermaus software with the coring site marked by black cylinder, b) black arrows shows groundwater terraces.

2.3. Geophysical measurements

The magnetic susceptibility and bulk density through the Asko-HT2017-2-GC core was measured by Multi-Sensor Core Logger (manufactured by Geotek, UK) in each 2 cm through all sections and used the PicoScope oscilloscope software and PicoLog data logging software to process these data.

A GEOTEK Multi-Sensor Core Logger (MSCL) measures different parameters such as magnetic susceptibility, gamma density and p-wave velocity (Figure 8). MSCL is fast and nondestructive, and gives high resolution analyzes.

2.3.1. Bulk density (Gamma density)

Before the gamma density measurement, a calibration was done with varying diameter aluminum in a water-filled core liner of a known thickness and density. The result of the calibration is shown in Appendix 3. The gamma ray attenuation system measures the sediment density by emitting gamma ray radiation through the sediment and detecting the amount of radiation passing through the sediments with a detector opposite of the ^{137}Cs gamma ray source (Figure 9). The more radiation can travel through the sediment, the less dense that sediment is.

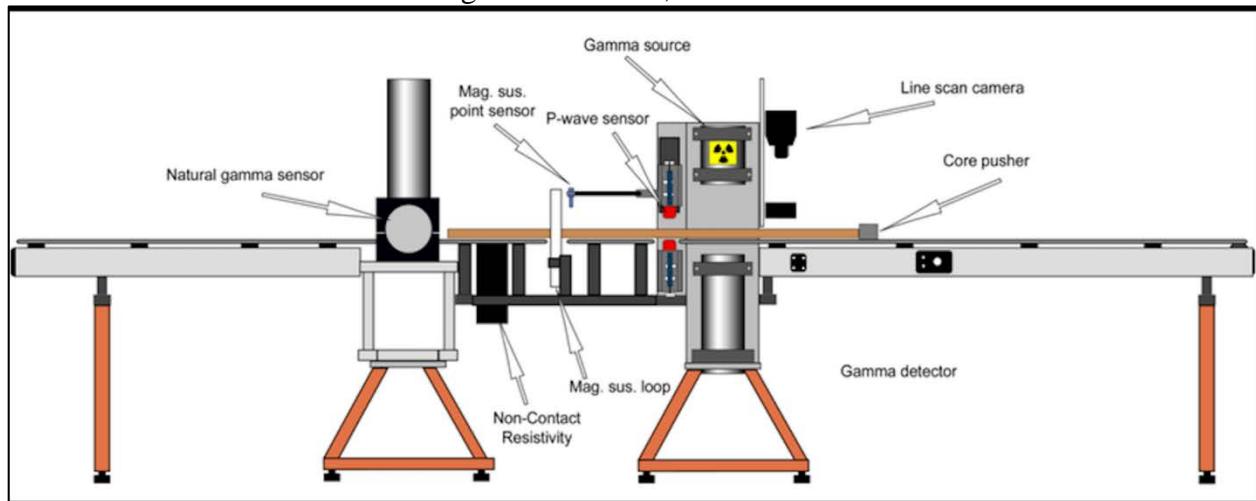


Figure 9. Multi-Sensor Core Logger illustration; retrieved from Lockhart, 2015.

2.3.2. Magnetic susceptibility

Magnetic susceptibility depend on the content of magnetic minerals in the sediments such as Magnetite. A magnetic susceptibility loop measures the magnetic susceptibility of the sediments by creating a magnetic field, taking away that field, and looking at how the sediments responded to the induced magnetic field.

2.4. Core description

Based on visual differences, the core has been divided into six distinct subunits. A description of each unit and their subunits is found below. The core is in good shape and the layering throughout the core is horizontal with hardly any disturbances. Some breaks in the core are seen

between 100 to 160 cm depth and also around 270 cm depth. The apparent grain size is silty clay gradually coarsening to clayey silt in the lower parts of the core (Figure 10).

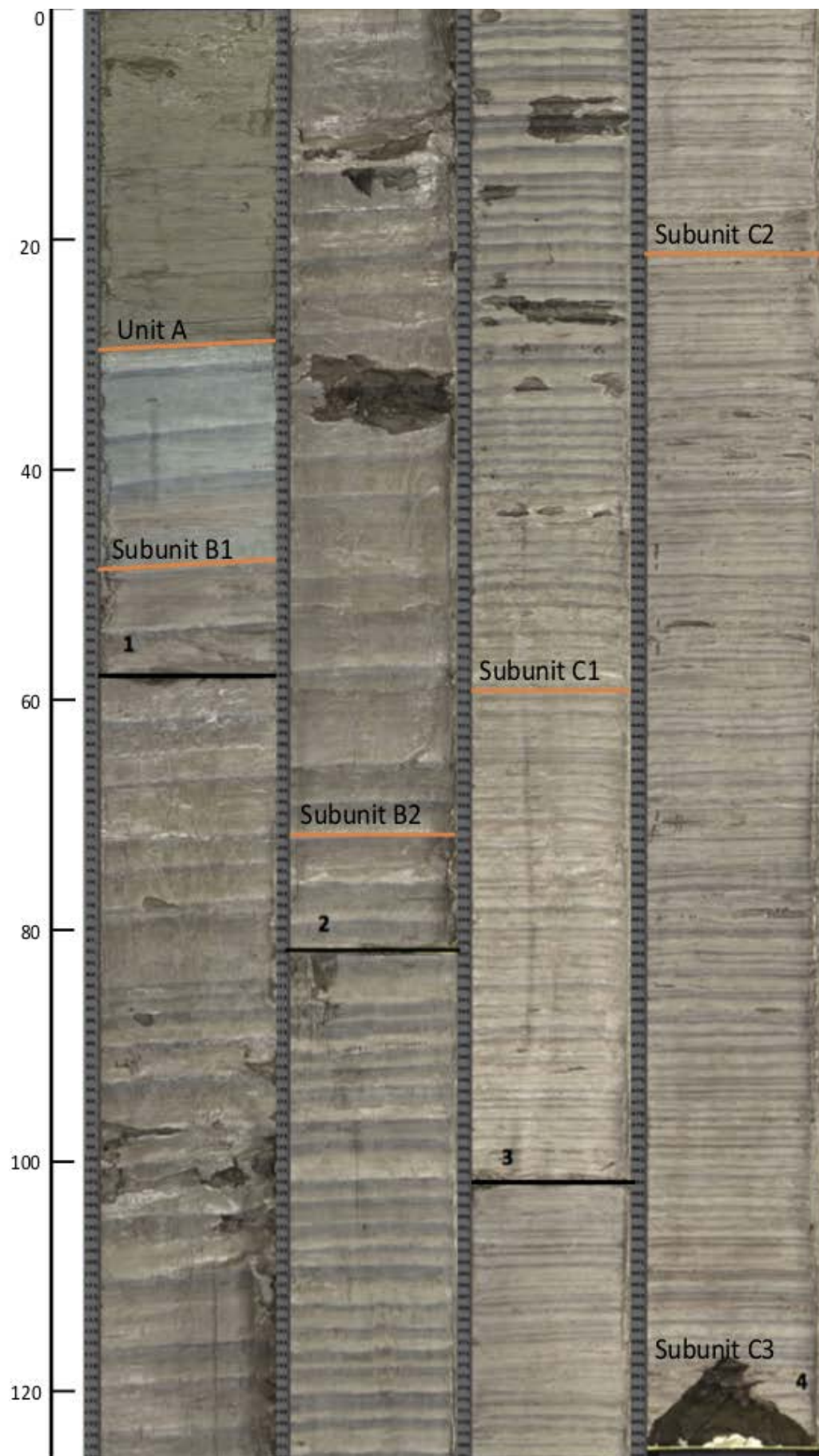


Figure 10. Photograph of the core Asko2017HT-02-GC which include four core sections; the uppermost section is number 1 and the lowermost is section 4.

2.4.1. Unit A

Unit A (0-31.5 cm depth) is homogenous fine-grained, silty clay with black mottling, brownish olive green to grey (Munsell: GLEY1 4/10GY). This layer contains around 1 mm thin and 2 to 3 cm long, almost black “mottles”. MSCL-logging shows magnetic susceptibility values of $6-7 \times 10^{-5}$ SI and a bulk density of 1.34 g/cm^{-3} within this unit. It is soft and “bouncy” in texture. This unit has a sharp basal contact with bluish-grey banded sediment.

2.4.2. Unit B

Unit A is non-layered opposite to unit B and C; there is a sharp transition between unit A and B with a tiny sand layer in between. Unit B has thicker glacial varves compared to unit C with a distinctive color changing come in between from bluish-darker brown color in unit B to lighter brown-beige color in unit C. Unit B divided into two different subunits, subunit B1 shows bluish colors with coarser sediment while subunit B2 has a dark brownish color with finer sediment. The more details of each subunit come below:

2.4.2.1. Subunit B1

Subunit B1 (31.5-48 cm depth) consists of a small section with clay, relatively thick (cm-scale) laminas and alternating in tone from dark to medium grayish blue. The sediment is marked by 4-6 cm long varve thickness that are graded from a light blue (Munsell: GLEY2 5/5B) through to a darker grey (Munsell: GLEY2 4/5B) with a sharp change back to light blue at its top. Subunit B1 has a gradual change in magnetic susceptibility from 9×10^{-5} SI to 39×10^{-5} SI. Similarly, the bulk density ranges from 1.4 to 1.73 g/cm^{-3} (Figure 11).

2.4.2.2. Subunit B2

This unit (48-198 cm depth) consist of light beige-brown layers alternating with slightly darker brown layers. The texture of this section is firm, compacted clays. Varve thickness in subunit B1 is similar to subunit B2 and has a thickness about 4-6 cm with different color from light grey (Munsell: 2.5Y 5/2) to a dark grey-brown (Munsell: 2.5Y 3/1). Some deformations in the form of holes is present in the sediment between 100 to 160 cm depth. The magnetic susceptibility remains at a relative constant $48-66 \times 10^{-5}$ SI. A similar trend is apparent for the bulk density; it increases slightly from 1.46 to 1.73 g/cm^{-3} .

2.4.3. Unit C

The third unit is distinguished by thinner glacial varves and lighter brown color compared to unit B. The alteration is gradual between unit B and C. Unit C is divided into three subunits based on grain size, magnetic susceptibility and bulk density variations and slight color change.

2.4.3.1. Subunit C1

Subunit C1 (198-335 cm depth) is a very fine-grained brownish-green sediment with distinct 1-2 cm varve thickness of differing color. The laminations decrease in size and have a lighter tone compared to unit B. The clay has a semi-graded light brown-green (Munsell: 5Y 6/1) to dark brown-grey (Munsell: 5Y 3/1) with a sharp boundary to the next. A general rise in magnetic

susceptibility to $42-79 \times 10^{-5}$ SI from Unit B2 is apparent. Bulk density also experiences a rise to a steady $1.45-1.83 \text{ g/cm}^{-3}$ (Figure 17).

2.4.3.2. Subunit C2

The subunit has a gradual transition to lighter and finer glacial varves (3 to 403 cm depth), silty-clay, it is towards the last subunit and gets a new lighter in color (Munsell: 5Y 6/1) in the lowermost parts with finer lamination. This unit contains varves that are darker brown in color (Munsell: 5Y 5/8). The varve thickness change downward from around 2 cm and become thinner almost to 1 cm in this subunit. Some breaks show between 260-280 cm depth. The bulk density is $1.63-1.81 \text{ g/cm}^{-3}$. Magnetic susceptibility increases from 59 to 77×10^{-5} SI.

2.4.3.3. Subunit C3

Subunit C3 (403-503 cm depth) consists of the most fine-grained thin glacial silty-clay varves than all other subunits. The varves in the lowermost unit thins out even more and is ≤ 1 cm thick throughout the unit till the end of the core, with even lighter color. These summer layers have a thickness variation between 0.4-0.7 cm with light greyish-green color (Munsell: 5Y 6/1) and winter layers thickness are about 0.1-0.3 cm with a brownish-red color (Munsell: 5Y 5/2). The core ends at a depth of 509 cm where there is a short 5 cm deformation due to the core catcher. A relatively similar bulk density value to subunit C1 of $1.59-1.93 \text{ g/cm}^{-3}$ is apparent. However, a decrease in magnetic susceptibility to $51-77 \times 10^{-5}$ SI is evident (Figure 17).

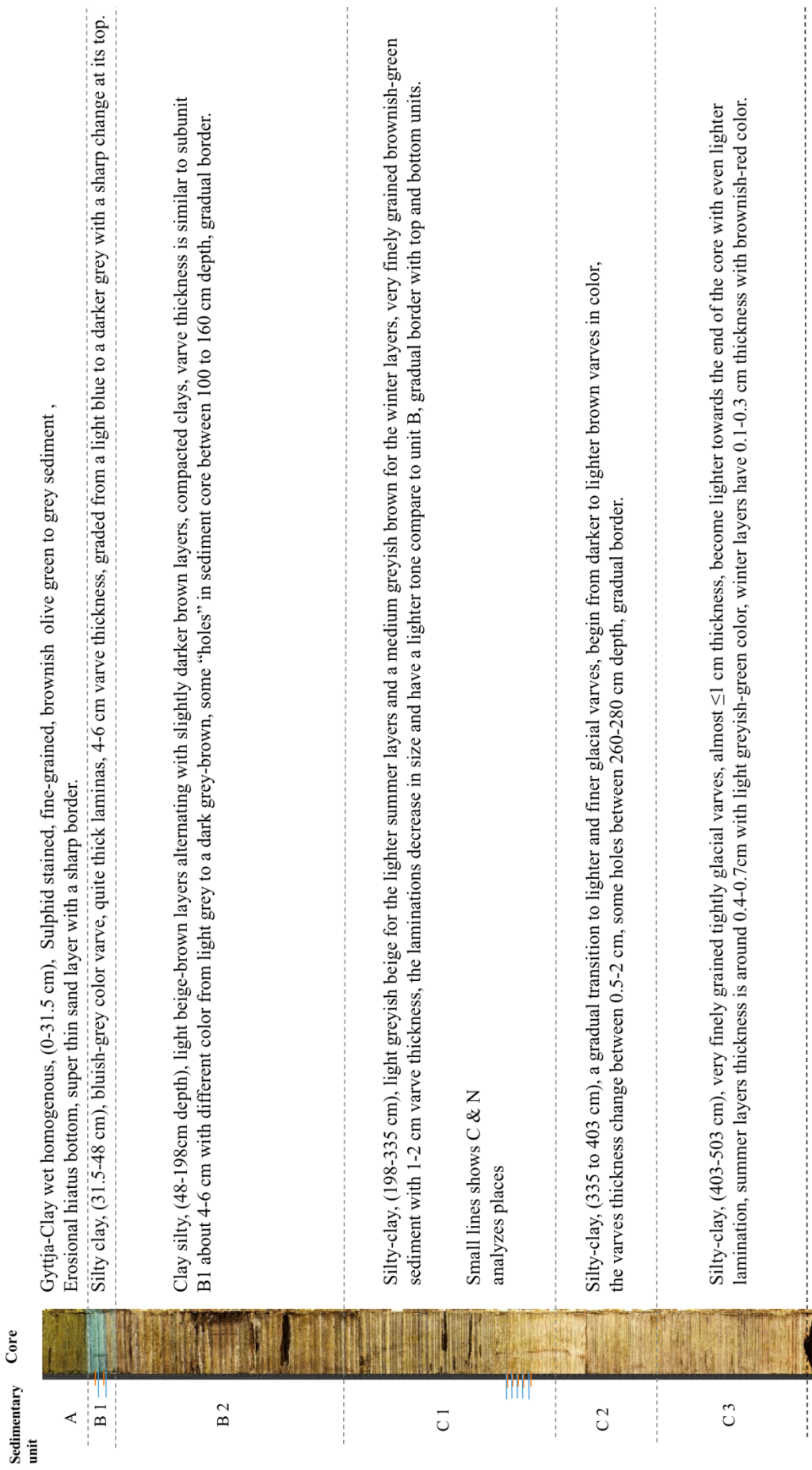
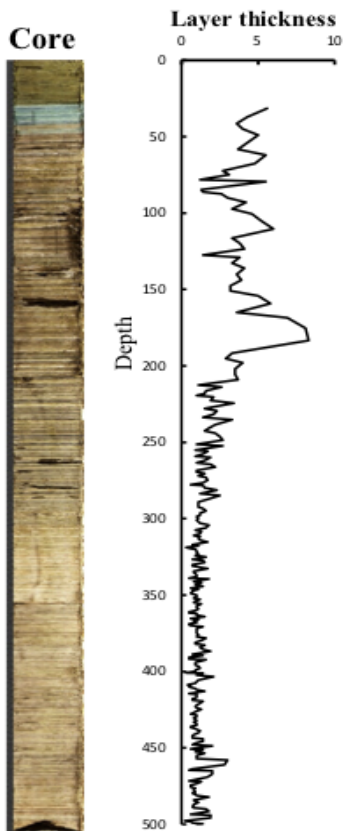


Figure 11: Core description and unit divisions.

2.5. Varve thickness measurement



After the core was split and scraped was digitally photographed in the MSCL. This digital imagery had a cm-scale next to the core which was used as a scale for varve counting. Each glacial varve consists of a light and a dark band. The beginning of each dark bands (winter layer) was counted downwards and its depth was noted in an excel file (top is zero). The varve thickness was measured by calculating the difference of all layer's depths. The varve thickness variability in cm plotted versus depth is shown in Figure 12. Note that this is not the same as the varve diagram in figure 16 because the varve diagram is plotted against varve number, and not depth. Based on De Geer's method these measured varves were plotted with the varve thickness on the Y-axis and the years on the X-axis. A local varve chronology from the southeastern Stockholm Archipelago has been done by Brunnberg in 1995. The new varve thickness graph is related with the located chronology in this area to estimate a distinct time span. As a result, a varve chronology has been provided for study area.

Figure 12. Asko2017HT-02-GC varve thickness plotted versus depth. This is not the same as the varve diagram in figure 16 because it is varve thickness plotted against the depth but the varve diagram is plotted against varve number.

2.6. Core sub-sampling

A total of 340 samples were taken from the core for grain size analysis, with different distances between each sample. The uppermost ~30 cm of the core that contained no visible glacial varves was sampled every 5 cm (Figure 10). In the varve parts, samples were taken from both summer- and winter parts of each sampled varve. Sample spacing was determined by varve thickness. In thick varves (~50 mm) several samples from the same varve were taken, and where varves were thin (~1 mm) only every fifth varve was sampled.

2.7. Grain size measurement

The grain size distribution was measured by Malvern Mastersizer 3000 at the Department of Geological Sciences, Stockholm University (Figure 13). This is a laser diffraction instrument which measures the grain size of any material from hundreds of nanometers up to several millimeters in size. When a light beam hits a particle, light is reflected, diffracted, refracted, absorbed and reradiated (Galacgac and Ooi, 2018). Analysis of small particles requires knowledge of real refractive index and imaginary refractive index but refractive index values are

less significant for large particles (Galacgac and Ooi, 2018). A laser beam passes through a sample in suspension and light is scattered from that sample. Particle size distributions are measured from the angular variation in intensity of the diffracted light from the sample. The angle and intensity of the scattered light depends on the grain size (Andrews et al., 2010). Larger particles scatter at smaller angles and more intensely while smaller particles scatter at wider angles and less intensely (Andrews et al., 2010). Scattering data typically cannot be inverted to find particle size but need different models to be interpreted. All calculations are handled by the Malvern instrument software. There are two different models to interpret scattering:

A: Fraunhofer diffraction: works best for large particles and the math is more straightforward. It does not require knowledge of the optical properties of the sample. If all particles are larger than the light wavelength and only scattering in the near-forward direction, then the fraunhofer approximation gives good results (Lebrun et al. ,1996).

B: Mie scattering: can be used for all particle sizes but it requires more complex calculations and knowledge of the optical properties of the sample. The nature of the input is important to decide a suitable wavelength; decreasing wavelength is the same as increasing size. Small particles appear bigger by shorter wavelength. Mie scattering is an exact treatment for spherical particles. Light scattering calculates the particle size distribution, assuming a volume equivalent sphere model. (Lebrun et al. ,1996).

This study uses the Mie theory which presents the best general solution for smaller particles size $< 50 \mu\text{m}$). The particles size in this study is almost just clay and silt particles ($>63 \mu\text{m}$) which in Fraunhofer approximation would give poorly results. Fraunhofer is simplified and does not account for optical properties in this analysis because in this model only scattering at the contour of the particle is considered; this also means that the same scattering pattern is obtained as for thin two-dimensional circular disks and only scattering in the near-forward direction is considered (Lebrun et al. ,1996).

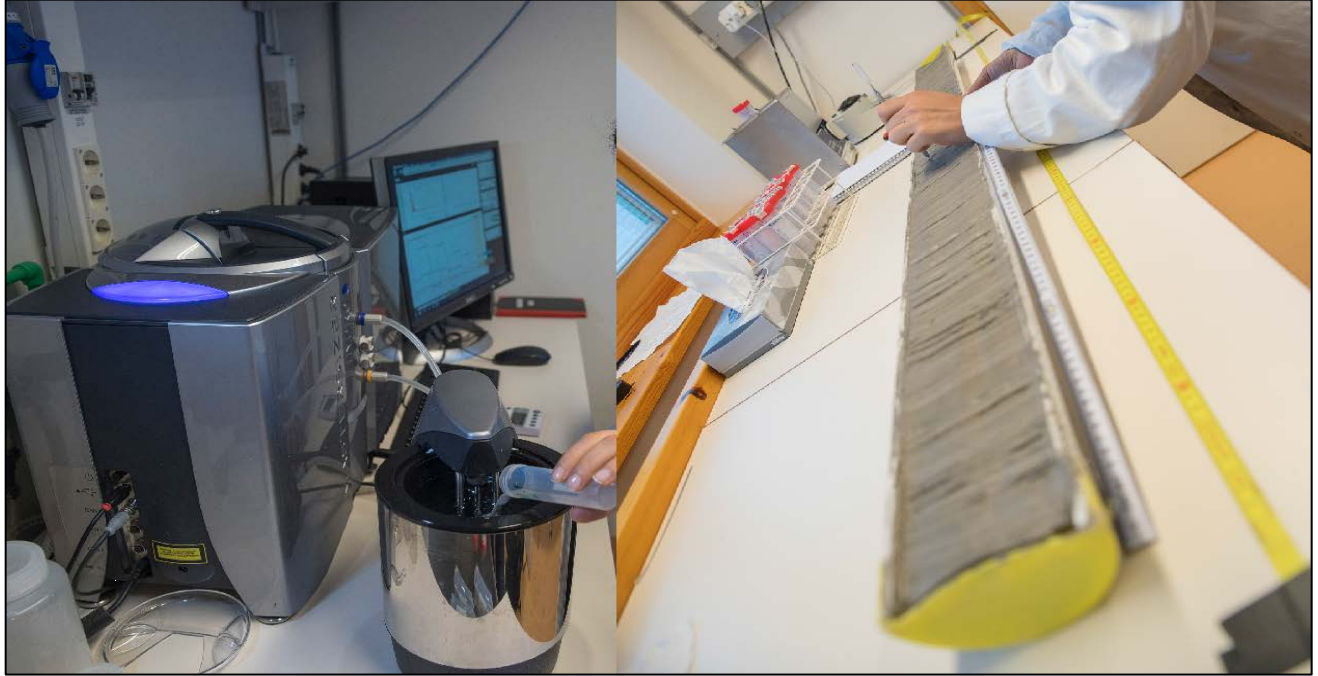


Figure 13. Sample preparation from Askö2017HT-2-GC-2 (right) for analysis in the Malvern instrument (left); sediment samples were scraped from the surface of the sediment core using a small spatula, across the entire surface and in parallel to the bedding.

Before sample analysis in Malvern, wet samples require preparation and dispersion. The first step is to initialize the system (alignment), then press start to begin the measurement. The background scattering signal from dispersant is recorded (Mastersizer 3000 User Manual, 2011). The background signal is subtracted, leaving zero scattering (and minor fluctuations), then the sample was added, and the scattering signal and obscuration increased as a result. Ultrasound was used to provide further dispersion, elapsed ultrasound duration was one minute for each sample. Then the measurement was started when obscuration was in range (5-12%). Five repeat measurements were processed for each sample and the average of these five measurements was obtained (Mastersizer 3000 User Manual, 2011).

2.7.1. Measurement procedure

The sample volume was just the tip of the spatula (Figure 13) and only wet sediment samples were used in this study. The sample was transferred to a small beaker and slurried in de-ionized water and mixed with dispersant, 3 ml of 10% sodium hexa-metaphosphate (NaPO_4)₆ was added by pipette to the deionized water in the sample container to avoid agglomeration (Figure 13). Since the sample container is automatically filled to 600 ml, the final concentration is about 0.05% in the Hydro LV measurement container. The operational details of this study is based on the standard operation protocol by Granberg (2012), as in Table 2. Even pure liquids scatter due to density fluctuations, there is often some constant background signal due to stray light. Detectors will always show a background signal, these effects are small, but they should be corrected. Big peaks in the background measurements mean particles or bubbles. Then the sample beaker was run in an ultrasonic bath for about one minute until all visible lumps had

disappeared, before it was poured into the sample container. After each measurement sequence, the system was thoroughly cleaned to be ready for the next measurement.

Stirring speed	3500 rpm
Pre-stirring duration	180 seconds
Measurement duration	30 seconds
Obscuration	5-12 %
Dispersion solution	deionized water + 3 ml 10 % (NaPO ₄) ₆ – solution
In sonication duration	60 seconds (during the first 60 seconds of pre-stirring)
In sonication level	100 %

Table 2: The Malvern Mastersizer 3000 standard operation.

2.7.2. Data export

Malvern Master size 3000 analyzes particles in 71 size classes, each covering 0.184 Φ . The data contains the % of grains in each size class. The phi scale is a logarithmic scale for grain-size. The millimeter and phi scales convert to each other by this formula: $\text{PHI} (\Phi) = -\log_2 S$ (Φ = the grain size in phi units, S= the grain size in millimeters) (Blott and Pye, 2001). Because the PHI classification of size scale was used by the software the size classes are larger for larger grain sizes ranging from 0.055 μm (smallest classes, fine clay) to 3500 μm (largest class, coarse sand). All records were exported as a text file and imported to Excel and the mean values from these replicate measurements were employed. Folk and Ward (1957) introduced a graphical method to estimate various statistical parameters of grain size distribution data which have only percentiles cumulative frequency (such as grain size distribution on Malvern). Statistical parameters such as sorting, skewness, kurtosis and mean were generated by using GRADISTAT Version 8.0 (developed by Blott, J. and Pye, K., 2001) for a better analyzing of the obtained grain size distribution data by Malvern. Grain size parameters in phi units (logarithmically) were used in this study. Since in GRADISTAT Version 8.0, it could be analyzed up to 250 samples together at once in "Multiple Sample Data Input" sheet and 340 samples were needed to be analyzed in this core, the obtained grain size data from Malvern were divided into two parts and measured in two times. In terms of graphical output, the program provides graphs of the grain size distribution and cumulative distribution of the data in both metric and phi units and displays the sample grain size on triangular diagrams. Samples could be analyzed singularly, or up to 250 samples together. The resulting statistics for all samples are summarized on an Excel sheet. The average of Mean, Sorting, Skewness, Kurtosis were calculated for all samples (Table 3b, c and d).

The particle size results were also divided into three classes which specified below: sand particles included all particles ≥ 4 at Φ scale ($63 \geq \mu\text{m}$), silt was between 4-9 at Φ scale (2-63 μm) and clay defined all particles < 9 at Φ scale ($< 2 \mu\text{m}$). All values within the Malvern size classes were added for sand, silt and clay respectively, i.e. the sum of all data bigger than 63 μm was classified as sand, data between 2-63 μm as silt column and all particles lesser than $< 2 \mu\text{m}$ as clay. For a more detailed analysis of transport energy or distance to the sources area. More detailed classification was made according to Wentworth's (1922) silt particles were classified in to four groups: very fine silt 4-8 μm , fine silt 8-16 μm , medium silt 16-31 μm and coarser silt 31-62 μm . In the same way sand particles were divided to five groups: very fine sand 62-125 μm ,

fine sand 125-250 μm , medium 250-500 μm , coarse sand 500-1000 μm and very coarser sediment considers for all particles between 1000-2000 μm (Figure 18). Since very coarse sand particle or gravels >1 mm is unreliable because of the small sample size, this group was not considered in this study. The data was plotted against depth in Excel, the vertical axis was displayed the depth (y axis) and the horizontal axis was showed grain size (x axis) with 3 various curves for sand, silt and clay particle and two diagrams for under grouping classification (Figure 17 and 18).

2.8. Carbon and Nitrogen methods

C/N analysis was made at 7 glacial varves, with a total of 14 samples, 4 samples from unit B1 (bluish gray varves) and 10 samples from unit C (where the color changes from gray to brown). Samples are taken from the core, then freeze dried and milled before weighing and analysis. Twice exemplified from each sample depth in core (cm); one for measure carbon content and the other one for nitrogen content (Appendix 2). They were weighed at 20 ± 5 mg (into tin cups for N content analysis and silver cups for C content analysis). All samples in silver cups were acid treated with hydrochloric acid (HCl) in oven at 60 °C overnight prior analysis to detect any occurrence of carbonates. Samples are combusted at 1020°C in a reactor packed with chromium oxide and silvered copper oxide. Following combustion, oxides are removed in a reduction reactor (reduced copper at 650°C). Carbon and nitrogen isotopes were measured but did not give reliable results because of too low organic content and that they will not be used in the thesis.

3. Results

3.1. Stratigraphy

The core indicated three distinct lithological units, labeled A, B, and C, where the lowermost unit (C) was divided into three subunits and the middle unit (B) was divided into two subunits. Some holes in the core are seen between 100 to 160 cm depth and also around 270 cm depth, most likely from splitting the core. Grain size generally varies between silty clay to clayey silt. Core depths between 31.5 – 335 cm are displaying distinct laminae, with dark and light alternating bands, clearly indicating glacial varves. There is a variation in glacial varve thickness. The varve thickness in unit B is between 4-5 cm while the varve thickness is thinner in unit C around 1-2 cm. The top of unit B shows bluish gray varves but continues to unit C with beige brown color which becomes lighter towards the lower end of the core. There is a gradual change between all units except the border between unit A and B1. There is sharp contact at the top of the Blue layer on unit B1 to greyish layer on unit A with a possible hiatus between. A thin sand layer lies on top of the blue varves (unit B1), which in turn is underlain by brownish olive-green sediment (unit A). The sand layer indicates erosion between the glacial varved clay and the post glacial clay (Figure 14). The silt and clay percentage in the grain size graph shows also a reverse trend at depth 335 cm (clay starts to increase and silt begins to decrease). There is a difference also between winter and summer layers as C org & N content increase above the 314.1 cm. The mean varve thickness also presents a new trend after this depth. The varves become thicker gradually upward after this depth (from 2 cm reach to 6 cm thick) but below this depth glacial varves are thinner (almost ≤ 1 cm).



Figure 14. Thin sand layer between the glacial varves in unit B1 and greyish layer on the top which display a hiatus between unit A and B.

3.2. Varve thickness measurement

The new varve thickness pattern was visually correlated to four previous Brunbergs varve-thickness data. By comparing the new varve thickness diagram with older varve thickness diagrams a suitable fit was obtained for core Asko2017HT-02-GC-1. The correlation obtained between the new varve thickness record and these four varve diagrams since they had the longest varve thickness record and their location were closest to the current core position (Figure 15).

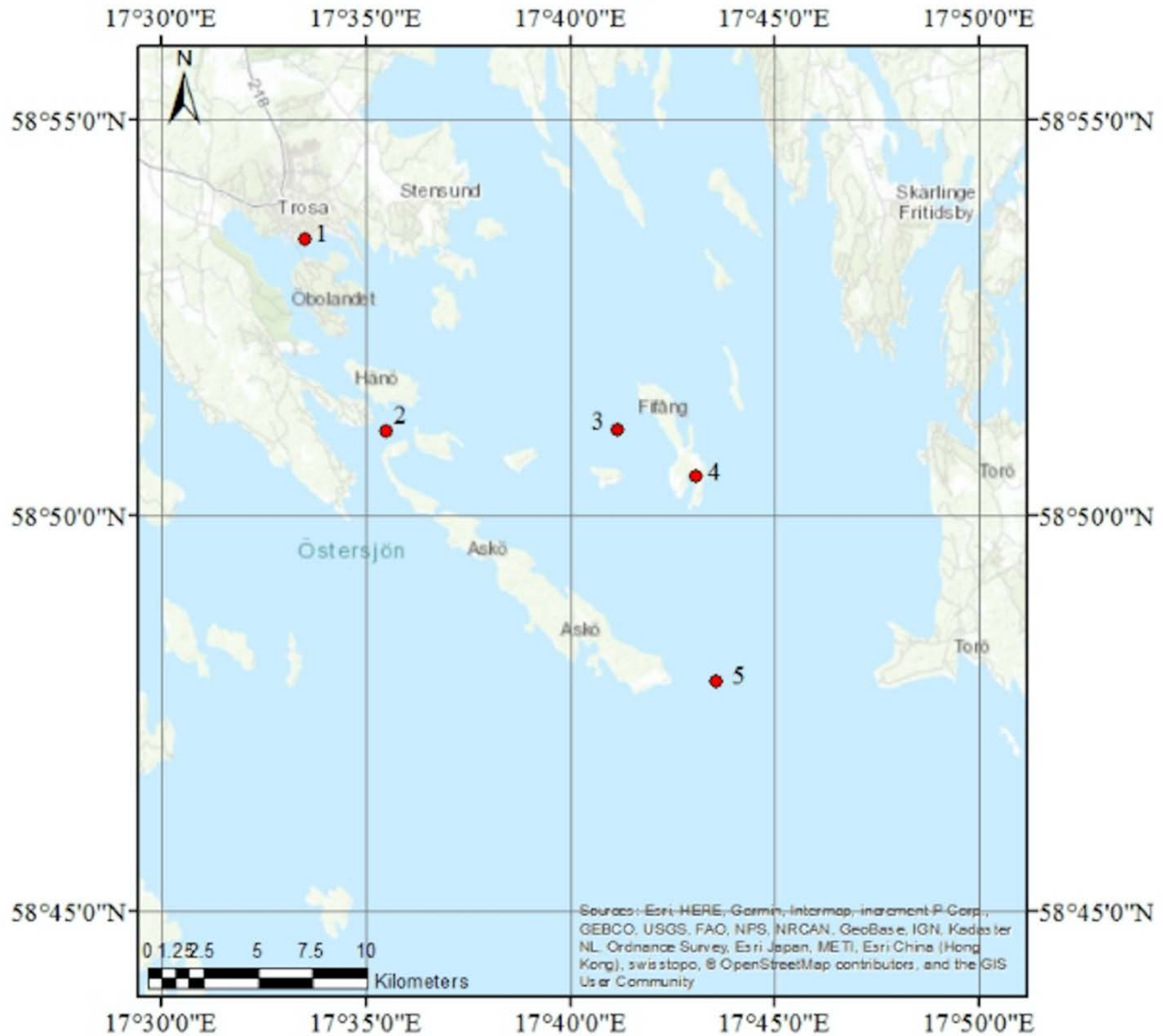


Figure 15: Core location (point 3: Askö 17) with the four nearest previous cores studied by Brunberg in 1995 which uses in this study; (1: Trosa, 2: Korsnäs, 3: Askö17, 4: Fifång and 5: Askö P5).

The basis for variation in the peaks and troughs of the varve diagram depend on the distance ice margin, the sediment transport energy, melt water amount and sediment availability. The Trosa varve-record had the oldest glacial varves in the Askö region (Brunberg, 1995). Since the age of Barenberg's varve-thickness diagrams were specified and the new core thickness diagram matched best as mentioned above, it obtained a new varve chronology. As a result, the new varve chronology excel file present a list of varve numbers which each varve number display a distinct year in a distinct depth. Figure 18 illustrate diagrams overlapping matched tie points between these records (Black dotted lines in figure 16).

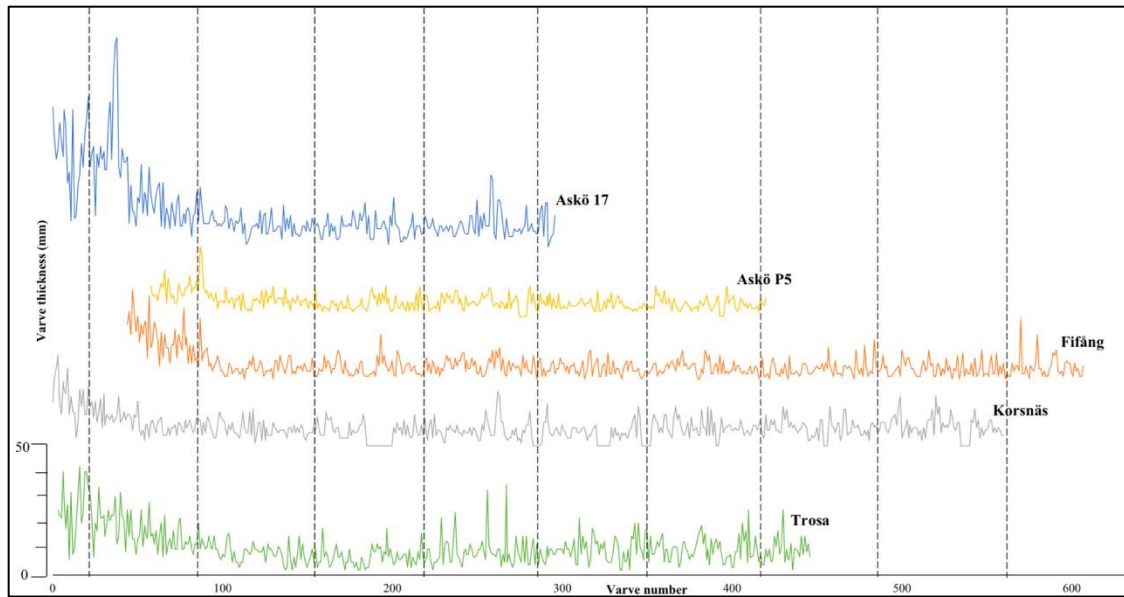


Figure 16. Plot of four previous varve records which correlated by the new varve thickness record (core Asko2017HT-02-GC-1). Black dotted lines illustrate some example tie points that used for correlation in these records.

3.3. Grain size, magnetic susceptibility and bulk density

There is a big difference between unit A and the rest of the units, as the highest silt and sand percent and the lowest clay percent display in this unit (sand 10%, silt 80% and clay 10%), as well as the lowest magnetic susceptibility and bulk density. Unit B have thicker varves compared to unit C. The sand percent decreases gradually from the beginning of subunit B1 until the end of the subunit B2 (from 10% to 0.08%). Magnetic susceptibility and bulk density increase rapidly in subunit B1 and continues slowly rising through subunit B2.

Unit C1 shows finer sediment (silt decrease from ca. 70% to 40% and clay increase from ca. 35% to 65%), magnetic susceptibility and bulk density increase very slowly. Unit C2 shows a coarser sediment trend than unit C1 (silt increase from ca. 40% to 70% and clay decrease from ca. 30% to 50%). It shows also a reverse trend at depth 335 cm (clay start to increase and silt begin to decrease). The difference also between winter and summer layers in C org & N content gets larger below 309.8 cm core depth (Figure 17).

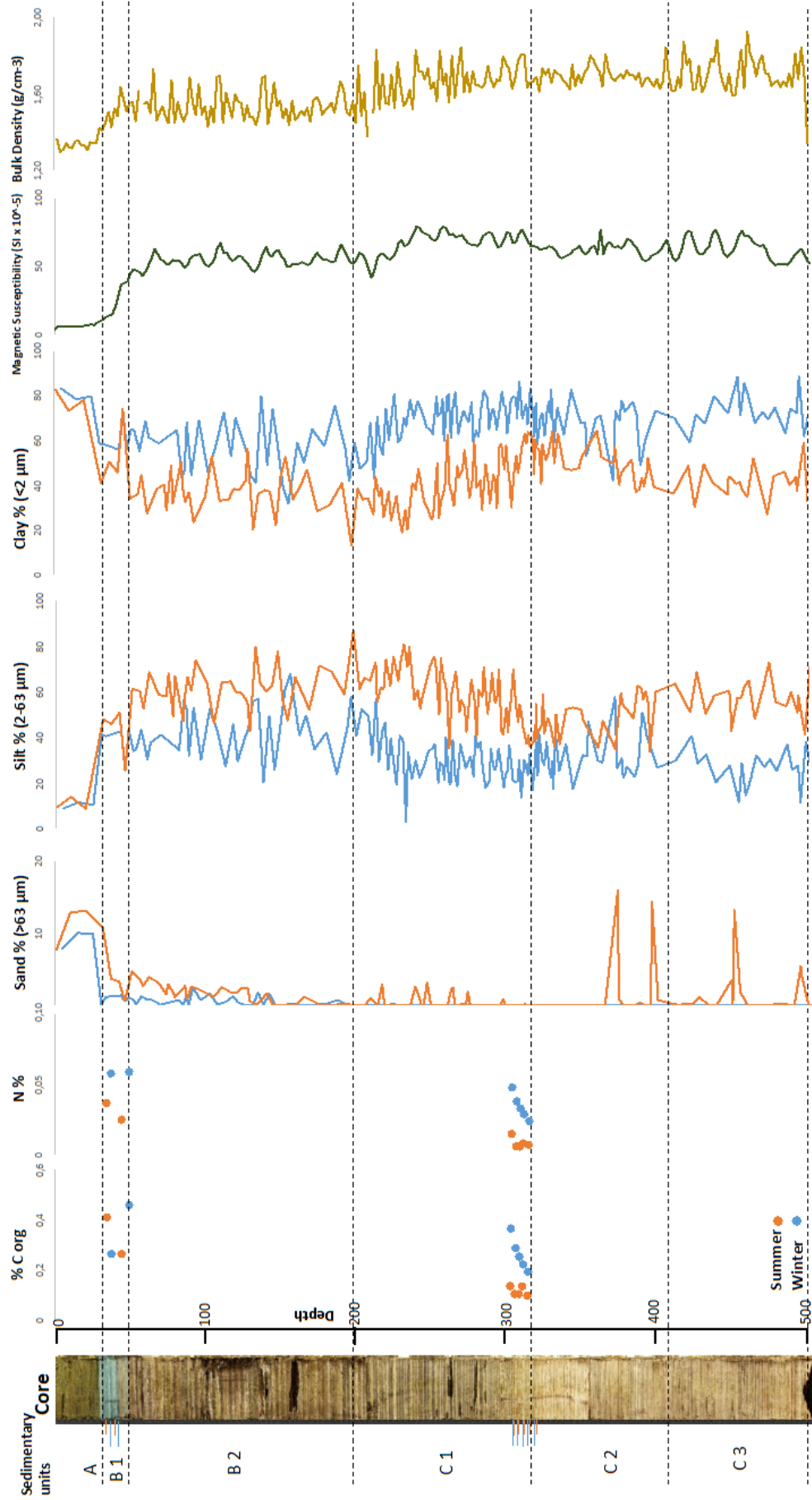


Figure 17. Core photo (with enhanced color saturation), unit division and measured parameters of core Asko2017HT-02-GC-1. Small horizontal ticks next to the core image shows location of samples for C & N analysis (orange is summer layer, blue is winter layer).

The mean varve thickness also presents a new trend after this depth (Figure 17). The varves become thicker gradually upward after this depth (from 2 cm reach to 6 cm thick) but are thinner below this (almost ≤ 1 cm).

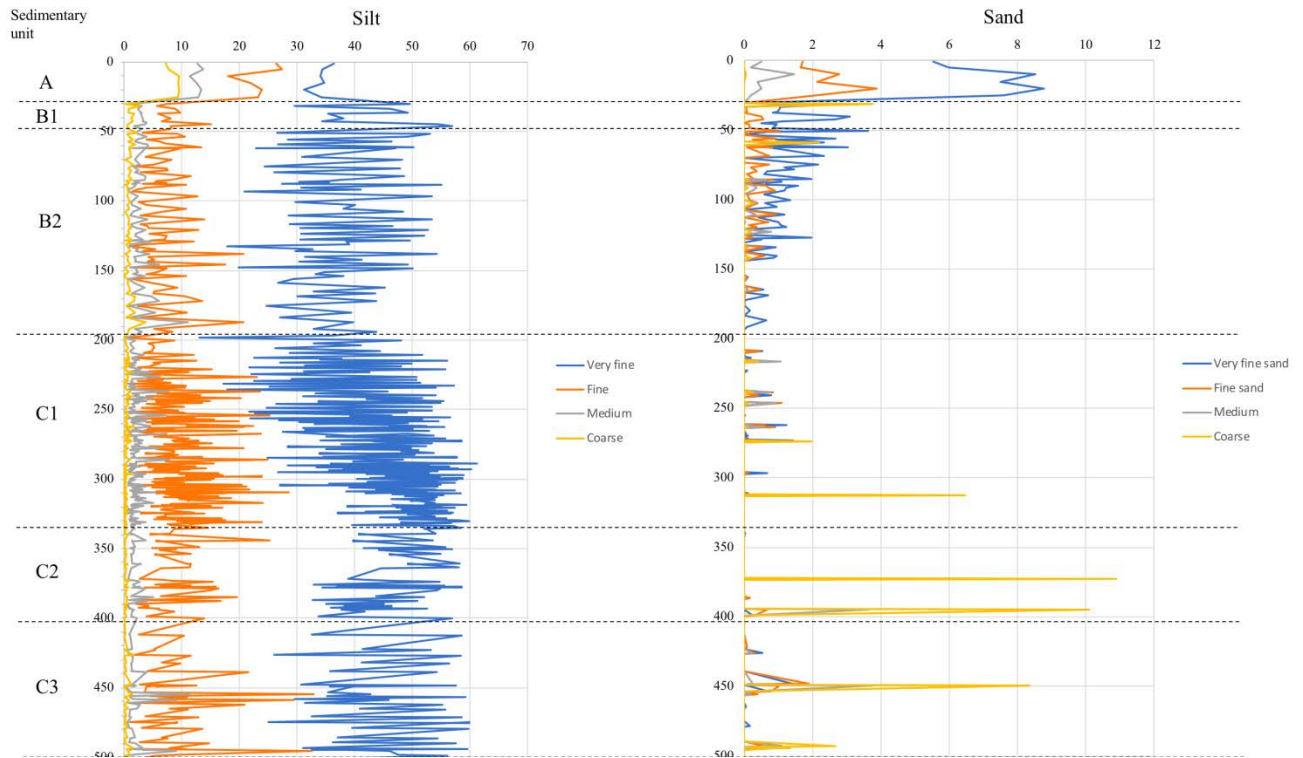


Figure 18. The grain size sorting distribution of core Asko2017HT-02-GC-1.

This graph shows the same trend as a lithology log in figure 17. Unit A display coarser sediments compared to rest the of the core. The distribution of silt and sand particles illustrate a poorly sort sediment, except unit A which has very poor sorting. The most dominant particle sorting groups display very fine silt and sand particles (blue color in figure 18).

Statistical analysis by GRADISTAT Version 8.0 in figure 20 shows the same trend as the grain size distribution by Malvern in figure 17. Table 3a display the average of all statistical analysis in phi scale (Logarithmic: Φ). Folk and Ward (1957) are suggested descriptive terminology for each classified grain size parameters group (Table 3a) and these descriptions were used to characterize in this study (Table 3d).

(c) Logarithmic method of moments

Mean	Standard deviation	Skewness	Kurtosis		
$\bar{x}_\phi = \frac{\Sigma f m_\phi}{100}$	$\sigma_\phi = \sqrt{\frac{\Sigma f (m_\phi - \bar{x}_\phi)^2}{100}}$	$Sk_\phi = \frac{\Sigma f (m_\phi - \bar{x}_\phi)^3}{100\sigma_\phi^3}$	$K_\phi = \frac{\Sigma f (m_\phi - \bar{x}_\phi)^4}{100\sigma_\phi^4}$		
Sorting (σ_ϕ)	Skewness (Sk_ϕ)	Kurtosis (K_ϕ)			
Very well sorted	<0.35	Very fine skewed	>+1.30	Very platykurtic	<1.70
Well sorted	0.35–0.50	Fine skewed	+0.43 to +1.30	Platykurtic	1.70–2.55
Moderately well sorted	0.50–0.70	Symmetrical	-0.43 to +0.43	Mesokurtic	2.55–3.70
Moderately sorted	0.70–1.00	Coarse skewed	-0.43 to -1.30	Leptokurtic	3.70–7.40
Poorly sorted	1.00–2.00	Very coarse skewed	<-1.30	Very leptokurtic	>7.40
Very poorly sorted	2.00–4.00				
Extremely poorly sorted	>4.00				

(d) Logarithmic (original) Folk and Ward (1957) graphical measures

Mean	Standard deviation	Skewness	Kurtosis
$M_Z = \frac{\phi_{16} + \phi_{50} + \phi_{84}}{3}$	$\sigma_I = \frac{\phi_{84} - \phi_{16}}{4} + \frac{\phi_{95} - \phi_5}{6.6}$	$Sk_I = \frac{\phi_{16} + \phi_{84} - 2\phi_{50}}{2(\phi_{84} - \phi_{16})} + \frac{\phi_5 + \phi_{95} - 2\phi_{50}}{2(\phi_{95} - \phi_5)}$	$K_G = \frac{\phi_{95} - \phi_5}{2.44(\phi_{75} - \phi_{25})}$

Table 3a. Statistical formula and suggested descriptive terminology modified from Folk and Ward (1957), Blott & Pye (2001).

All units except unit A display chiefly a poorly sorted sorting, coarse skewness, mesokurtic and mean between clay to very fine silt (Figure 20). Unit A shows very poorly sorted sediment, symmetrical skewness, leptokurtic to mesokurtic and in average medium silt particle (Table 3b). There are differences between summer and winter layers (Table 3c). Winter layers generally represent at average clay particle, poorly sorted, coarse skewed distribution and platykurtic kurtosis. Summer layers show instead very fine silt, poorly sorted, symmetrically skewed and mesokurtic (Table 3c).

Sample statistics unit A	No layers
Mean (\bar{x}_ϕ):	Medium silt
Sorting (σ_ϕ):	Very poorly sorted
Skewness (Sk_ϕ):	Symmetrical
Kurtosis (K_ϕ):	Leptokurtic - Mesokurtic

Table 3b. Statistical analysis of unit A.

Sample statistics units B & C	Summer layers	Winter layers
Mean (\bar{x}_ϕ):	Fine silt to very fine silt	Clay to very fine silt
Sorting (σ_ϕ):	Poorly sorted	Poorly sorted
Skewness (Sk_ϕ):	Symmetrical	Coarse skewed
Kurtosis (K_ϕ):	Mesokurtic	Platykurtic

Table 3c. Statistical analysis of unit B & C.

Average of all statistics analysis	Logarithmic (Φ)	Description
Mean (\bar{x}_ϕ):	8.643	Very fine silt
Sorting (σ_ϕ):	1.435	Poorly sorted
Skewness (Sk_ϕ):	-0.448	Coarse skewed
Kurtosis (K_ϕ):	3.174	Mesokurtic

Table 3d. The average of statistical calculation of grain size parameters in phi units for the whole core.

Figure 19 describe suggested terminology of statistical grain size distribution curve (Krumbein & Pettijohn, 1938 and Folk & Ward, 1957). Platykurtic has a low degree of peakedness (negative) while leptokurtic a high degree of peakedness (positive) and mesokurtic kurtosis has a normal distribution (zero). A positive skew has most values on the left of the mean but a negative skew has most values on the right side of the mean and a zero skew represent a symmetrical distribution (mean=mode=median).

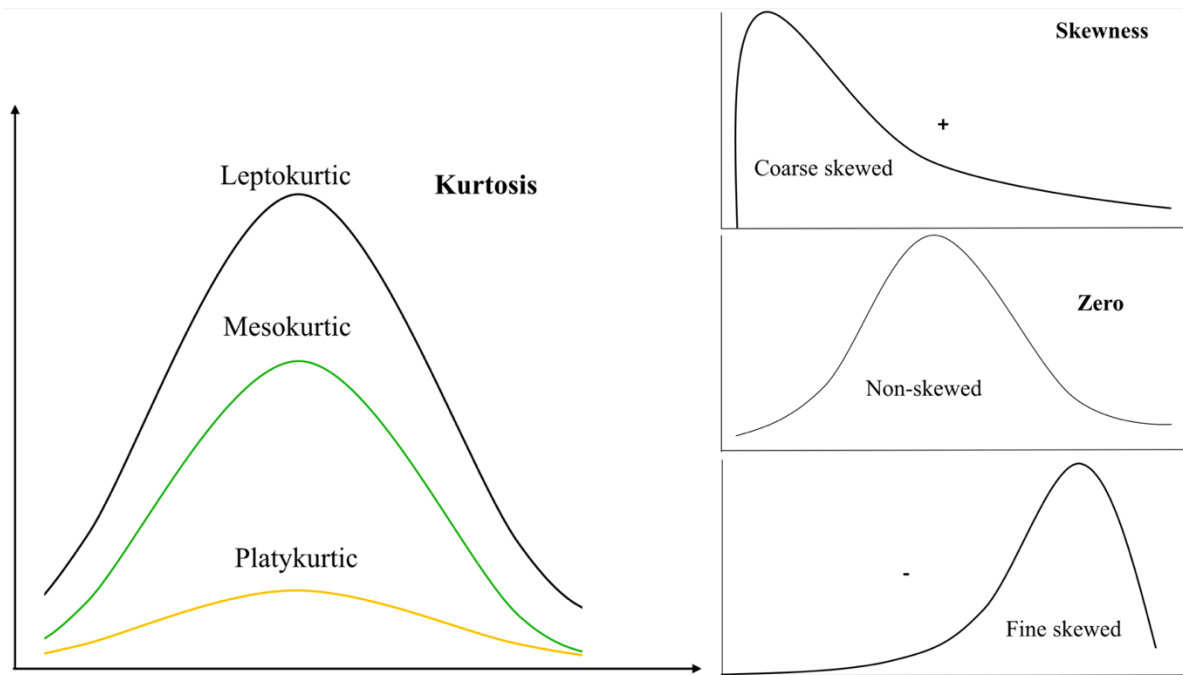


Figure 19. Illustration of the skewness and kurtosis values.

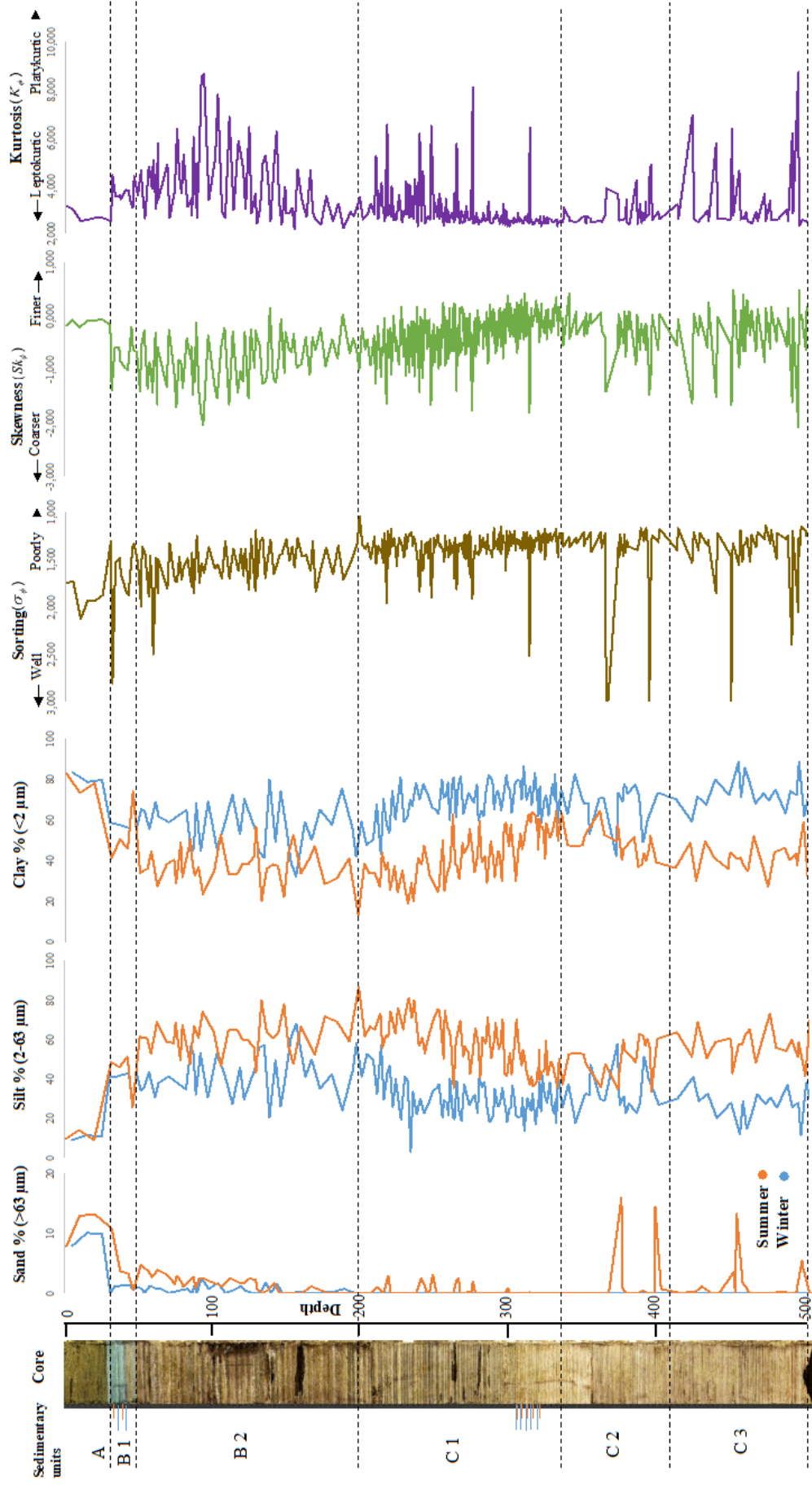


Figure 20. Core photo (with enhanced color saturation), unit division, measured grain size and statistical parameters (sorting, skewness and kurtosis) of core Asko2017HT-02-GC-1. Small horizontal ticks next to the core image shows location of samples for C & N analysis (orange is summer layer, blue is winter layer).

3.4.Organic carbon and nitrogen

Fourteen samples were taken for total carbon and nitrogen analysis. One sample from the winter layer and one sample from the summer layer in seven selected glacial varves (Figure 21). Four samples were from unit B which display blue color and ten samples from unit C, five samples were from greyish-brownish varves, and five samples from red-brownish varves (Table 4). As it was mentioned above each varve got a specified age at a certain depth. Table three display the sample depth in core by estimated age for each organic carbon and nitrogen sampling.

Varve number (top is zero)	Age (cal yr BP)	Sample depth in core (cm) for summer layer	Sample depth in core (cm) for winter layer
2	11489	34	37.1
4	11491	44	48.5
102	11589	302.5	303
104	11591	305.5	306
106	11593	308.2	308.5
108	11595	310.5	311
112	11599	314	315.3

Table 4: Varve samples depth (summer- and winter layer depth). Varve number and estimated age retrieved from figure 10 and appendix 1.

The organic carbon increases from 0.1% - 0.2% in unit C2 to 0.2–0.5% and in unit C1. Both C2 and C1 winter sample show higher values of organic carbon content.

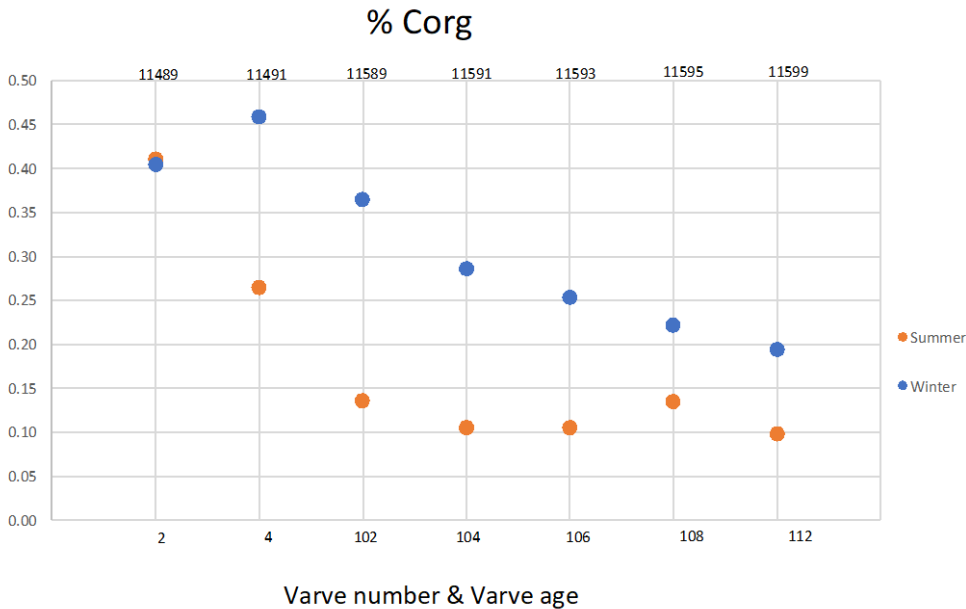


Figure 21. Organic carbon content in selected summer- and winter layers.

The nitrogen content percent shows the same pattern as the organic carbon percent (Figure 22). The C1 varves have a higher total nitrogen content (ca. 0.03-0.06) than the C2 varves (ca. 0.005-0.03). Winter samples from both C1 and C2 shows higher values of nitrogen content.

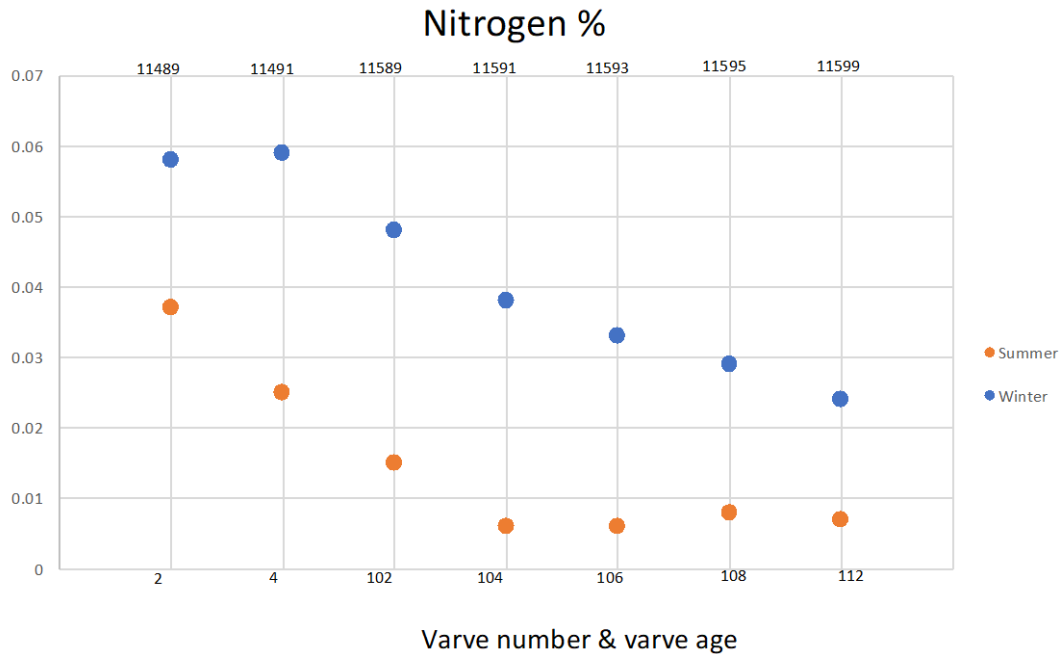


Figure 22. Nitrogen content in seven selected summer- and winter layers.

4. Discussion

4.1. stratigraphy

These parameters were investigated in this study: grain size, organic carbon content, nitrogen content and varve thickness. The parameters show a distinct pattern through each unit. The basic theory of glacial varve formation is that warmer temperatures gives more meltwater from the glacier, and more sediment deposition, and gives thicker varve layers. Cooler temperatures give less meltwater from the glacier and therefore less sediment and gives thinner varve layers. A couplet of a dark and a light layer is called a glacial varve, which corresponds to deposition throughout one year. Coarser sediments such as sand and silt are deposited mostly during the summer but during the winter when the melting stops, mostly clay particles settle. Winter layers is generally thinner and darker than summer layers (Lowe and Walker, 2014).

The varve thicknesses vary rhythmically throughout the whole core. There is unevenness in varve thickness due to length of the melt season or the summer. If one year is slightly cooler there won't be as much melting water and less sediment would be deposited. The thinner glacial varves in the bottom of the studied sediment core have almost equal thickness in summer and winter layers, but there is a trend with thicker summer layers and thinner winter layers towards the top of sediment core with beginning of the Holocene.

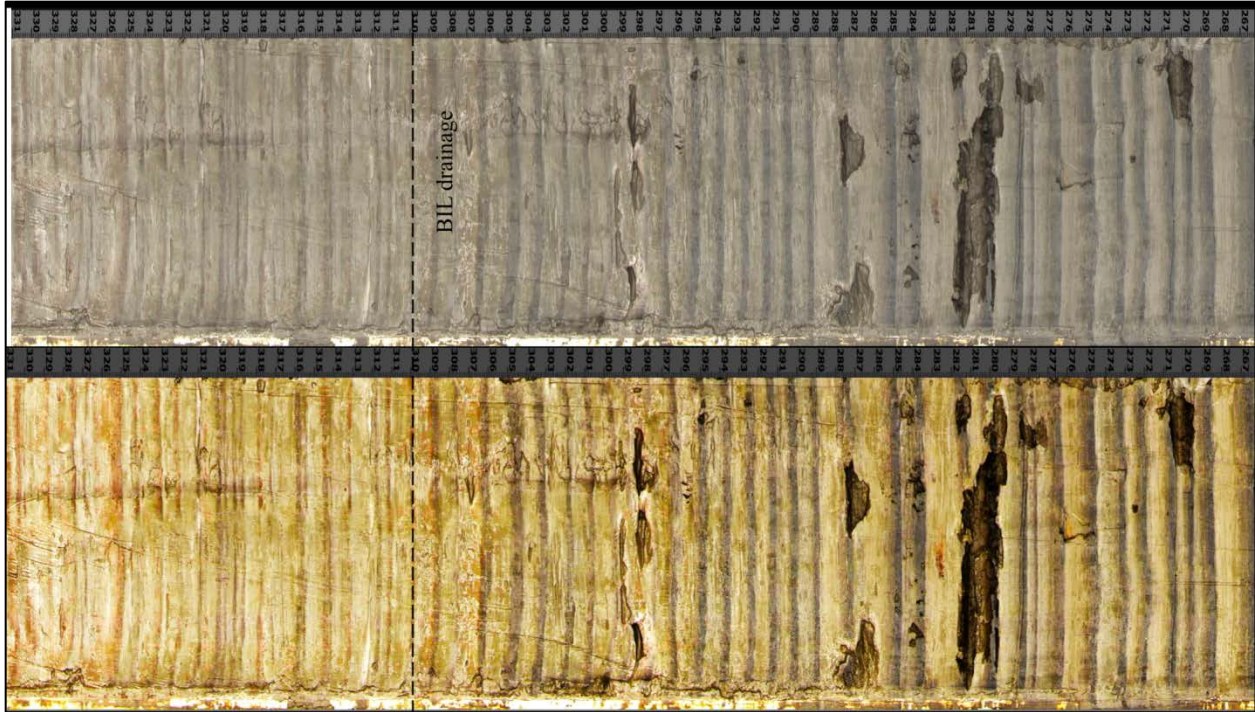


Figure 23. The BIL drainage depth which considered in this study. The color changes are more obvious in the lower images which has a higher contrast for better perception.

Figure 23 display these three changes which considered the BIL drainage compare to the most recent estimates in the scientific literature. First the color changes begins at this depth (to dark brown in the winter layers). The color reveals information about the mineral content (Wessels,1998). Second the varve thickness increases after this depth. Third the sediment becomes coarser after this depth (Figure 17) which represents a higher flow energy condition. The third reason correspond exactly by the new varve chronology which obtained for core Asko2017HT-02-GC-1.

4.2. Varve thickness diagrams

This core shows 299 varves. The varve thickness diagram for core Asko2017HT-02-GC-1 is connected to the Swedish time scale (STS) based on comparison with the four nearest varve diagrams Askö P5, Fifång, Korsnäs and Trosa, as measured by Brunnberg (1995) (Figure 16). Based on the connection to Barenberg’s (1995) diagrams from the Askö area, these varves were deposited 1398-1697 in the Swedish Time Scale (STS). The STS is the original time scale established by De Geer (1884), who proposed a key varve as a “zero-year”, older varves than the varve ± 0 got negative values (glacial varves) and varves deposited after the zero-year counted positive values (postglacial varves) (De Geer, 1884). The STS (the De Geer time scale) was connected to the present by Cato (1987). According to Cato, the zero-year varve coincide with 9240 varve yr BP relative to 1950 BP. A new varve timescale was suggested by Stroeven et al. (2015) based on correlation between the STS and the Greenland ice core record, where the zero-year varve is considered as ca 10090 cal yr BP. Following Stroeven et al. (2015), the years 1398-1697 STS equals 11488-11787 cal yr BP (10638-10937 varve years BP in Cato’s (1987) timescale) (Fig. 24 and appendix 1).

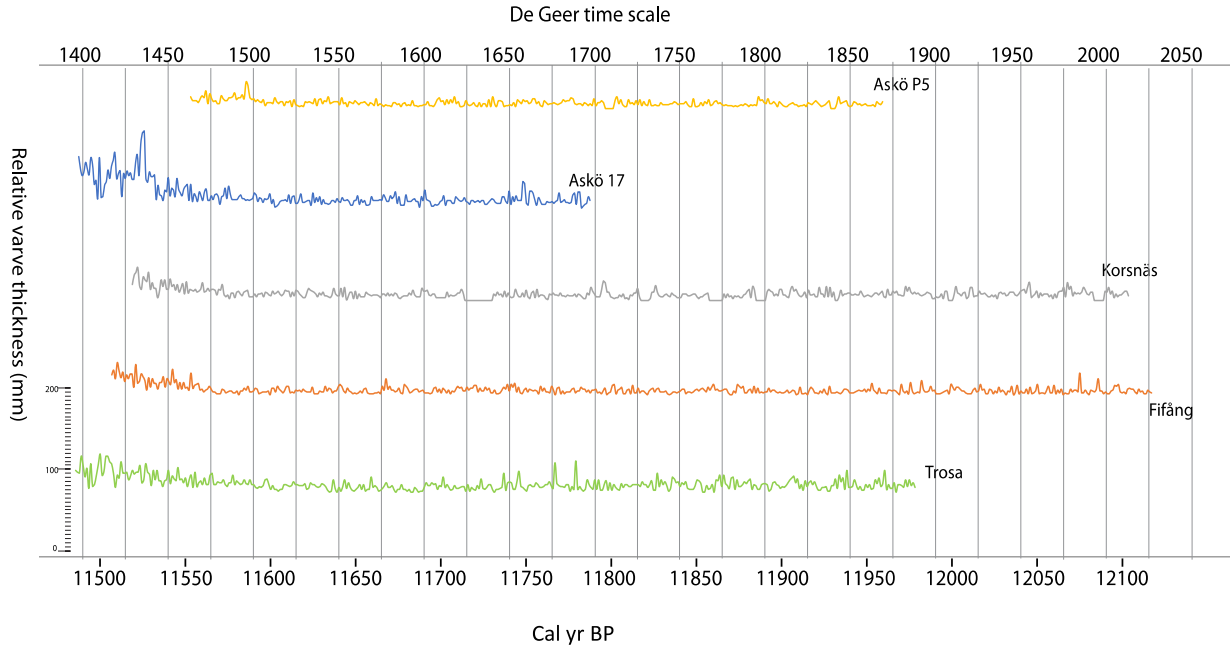
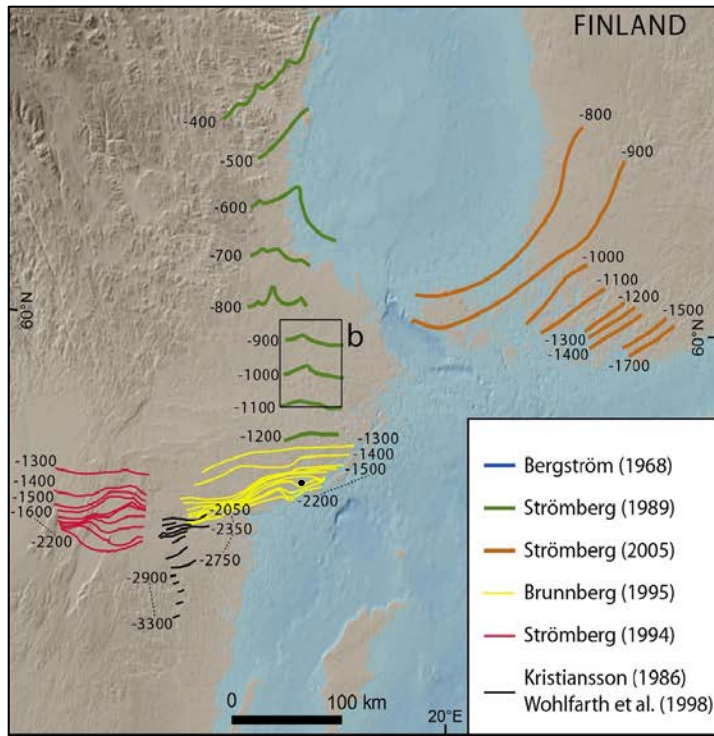


Figure 24: Varve thickness curves from the Askö area. The varve diagram for core Asko2017HT-02-GC-1 is labeled Askö 17.

Stroeven et al, (2015) estimated that the final BIL drainage occurred 11620 ± 100 cal years BP. Since the first varve in this core was deposited 132 years earlier at 11488 cal y BP then BIL drainage would be expected to occur in varve number 132 from above which is in 334 cm depth. Based on Andrén et al., 1999, a color change was recorded after the final BIL drainage and varve thickness increased afterwards. But no color change discernible by the naked eye is occurs at this depth in core Asko2017HT-02-GC-1. The BIL final drainage has been dated different in previous studies; Brunnberg (1995) estimated 10740 varve-years BP, Andrén et al, (1999) 10690 varve-years BP or 11480 cal y BP, and Andrén et al, (2002) 10770 varve-years BP or 11560 cal yr BP.

There is a change in color from beige to brown varves (from old to young) that begin from varve number 107 at depth 309.8 cm at the border between unit C1 and C2 in this core. Since the connection to the Greenland ice core record has an error margin of ± 100 (Stroeven, 2015), the age of the BIL drainage ranges from 11520 to 11720 cal yr BP. It is therefore reasonable to assume that the observed color change at 309.8 cm depth in core Asko2017HT-02-GC-1 represents the final BIL drainage, which corresponds to 11594 cal years BP.

Varved clay was deposited in front of the receding ice margin and the core position located just after the ice recession line -1900 which has been correlated with the STS by Brunnberg at 1995 (Figure 25). The ice front coring site (1700 line) was ca 12 km away from the beginning of varve deposition in this core and 27 km away coring site (1400 line) at the end of varve deposition in this core.



Varved clay was deposited in front of the receding ice margin and the core position located just after the ice recession line -1900 which has been correlated with the STS by Brunnberg at 1995 (Figure 25). The ice front coring site (1700 line) was ca 12 km away from the beginning of varve deposition in this core and 27 km away coring site (1400 line) at the end of varve deposition in this core.

Figure 25: Ice margin positions based on clay varve records in central Sweden. The coring location for Asko2017HT-02-GC-1 is indicated with a black dot on the yellow line -1900 in the map, and this implies that the coring site became ice free at ca 11990 cal yr BP. Modified from Stroeven et al, (2015).

4.3. Grain size, magnetic susceptibility and bulk density

The core location lie in a higher area than the surrounding seafloor, and no evidence of groundwater seepage was observed in this core. Therefore, the probability of the encountering a perched water table is lesser at this depth of coring. In addition, geophysical data display no significant groundwater escape features at the core location place. The sub-bottom profile (Figure 7a and b) illustrates a stratified acoustic unit with high contrast impedance in the most part of the core penetration depth. On the other hand, the grain size analysis in Malvern shows the grain size distribution silty clay and clayey silt (Figure 17). The distribution of silt and sand particles illustrate generally a poorly sorted sediment except unit A which shows a very poor sorting, the most dominant particle sorting groups display very fine silt and sand particles (blue in figure 18).

Statistical analysis by GRADISTAT Version 8.0 was given generally information about the transport and depositional sedimentary environments (source area). Statistical treatments of grain size data such as mean, sorting, skewness and kurtosis has been used in phi scale to make units of equal value in this study (Figure 20). Primary properties of sedimentary structures are largely controlled by the distribution of facies, which is in turn controlled by the depositional environments and grain size distributions (Beard and Weyl, 1973). Average and dominant texture of all 340 samples in this core shows generally very fine silt by poorly sorting sediment. The core average skewness -0.448 phi was classified as a coarse skewed in table 3d based on Folk and Ward (1957). Statistical analysis by GRADISTAT Version 8.0 shows the same trends as the particle size distribution analysis (Figure 17 and 20). During the summer when the energy of transporting is higher, coarser particle (fine silt to very fine silt) deposits mostly compared to finer winter layers sediment (clay to very fine silt). A symmetrical skewness (positive to low negative skewness value) display on the summer layers compared to a more coarse skewed

distribution in the winter layers, and finally a mesokurtic distribution shows on summer layers compared to platykurtic kurtosis on winter layers. These parameters represent a higher transport energy condition for summer layers compared to winter layers. Depositional processes were settling from suspension on winter layers which created a platykurtic kurtosis (a bigger range of sediment particle size) and ice meltwater deposition for summer layers which formed a mesokurtic (more the same sediment particles). Grain size deposition correlates to stream energy level for example if sediments are deposited near an ice margin, the sediment does not have enough time to become a well sorted before it settles. Low transport energy in winter is represented by finer particle size in this core (clay particles), platykurtic and coarse skewed distribution which means that chiefly suspension particles deposited through this season (Figure 20). There are also differences between these parameters in unit A and the rest of the core (units B and C). Unit A has symmetrical skewness and leptokurtic – mesokurtic distributions which describe deposits with a high degree of textural reworking. This unit has also the coarsest sediment (medium silt) and very poor sorting which could be explained by ongoing erosion on the seafloor. The thin sand layer in lowermost unit A and uppermost of unit B1 is distinct to both of these units, as it is leptokurtic (chiefly sand particles) and very coarse skewed and a better sorted compared to older and younger units. These analyses matches well with the grain size distribution which was interpreted as a erosion hiatus between unit A and B.

Units B and C have generally finer sediments (finer silt in summer, changing to clay in winter in units A and B compared to medium silt particles in unit A) and display better sorting than unit A (poorly sorted compared to very poorly sorted in unit A) and also shows milder kurtosis (from mesokurtic in summer layers and platykurtic in winter layers to leptokurtic-mesokurtic in unit A). These factors can be characterized by sediment deposition a longer distance from the ice margin. Generally, sediments sorting improves along the sediment transport paths. Since these sediments in unit B/C are poorly sorted, they have not been transported very far from their source (ice margin). Poorly sorted sediments demonstrate a wide range of particle size (Figure 20) in these units A and B. Unit B shows generally larger variance in its statistical parameters (mean, sorting, skewness and kurtosis graphs) compared to unit C, which means the data are very spread out from the mean on unit B but it is closer to the mean on unit C. Unit B illustrates a higher kurtosis, lower skewness and a better sorting compared to unit C. These parameters could be explained by a higher deposition rate and as a result of a warmer climate compared to unit C.

According to Beard and Weyl (1973) the whole core represents high porosity materials since the median of particles is between 16 -2 μm diameter (fine silt to clay) and poorly sorted (Figure 20). Permeability is controlled by both grain size and sorting. Fluid flows through the pore network between grains. Void space fraction plays a bigger role than the grain size (Beard and Weyl, 1973). Both silt and clay have low permeability, but usually, the larger grain size (well sorted), the better the porosity and permeability. If the materials are poorly sorted then the porosity and permeability would be reduced consequently because smaller particles filler between larger particles and reduce void space and flow paths, such as a sand and clay sediment mixture. On the other hand, clay has higher porosity because clay has a more surface area than sand, therefore, more water can be retained in the clay sediment. Based on Beard and Weyl (1973), unit A, which is dominated by medium silt and is very poorly sorted has a 30 % porosity, and unit B and C which are dominated by fine silt to clay and are poorly sorted has 34 % porosity. The force of molecular attraction in clay is high and it do not allow water move through the pore spaces

easily. Although, clay deposits have high porosity, but because they have little permeability, they do not form groundwater aquifers, despite the large volume of water they may contain, and are considered as an impervious material. Since the unit A has higher permeability (medium silt), water can move downward by gravity through this unit into lower layers. The pore space connection in clay is low and clay tends to hold more water. As a result water moves slower downward through unit B and C.

In sandy sediments, the adhesion is assumed to be approximately zero. The sand layer between unit A and unit B has a potential for groundwater flow. The previous investigation in this region illustrate terraces as a signs of ground water leakage and the second sampling core was obtained from a terrace area.

The grain size data shows different trends throughout the core. Unit A has the coarsest sediment in this core without any lamination, which could be a further evidence of ongoing erosion of the seafloor. The core location lies in a higher area than the surrounding seafloor and therefore is more exposed to erosion. According to the Blott & Pye (2001) unit A is classified as silty clay unconsolidated sediment. Unit A has a different acoustical signature from the underlying units which are more compact, layered sediments. Since the Swedish archipelago uplift ratio is higher than global sea level rise, an active sediment accumulation system on the bottom of the seafloor formed there. Smaller particles such as clay washed out and was transported to the deeper places (eroded) and as a result bigger particle such as sand and silt remained. Unit A also contains 1-2 cm long sulphide black mottling which is common in gyttja clay (organic clay).

The first down core particle size change start at 31.5 cm depth in bottom of unit A, where the youngest glacial end. Unit B begins with a large alteration in grain size. Finer sediment in this unit demonstrate a cooler climate compared to unit A. The sub bottom profile represents three different units where the, first acoustic unit is interpreted as post glacial clay, the second display a stratified acoustic unit which demonstrate varved glacial clay (corresponding to the stratigraphy in this core) and finally the third acoustic unit represent the bedrock. The sand amount decreases from 10-12% in unit A to 3-0% in unit B and the silt amount is reduced from 85-75 % in unit A to 45-55% in unit B, whereas clay increases from ca 10 % in unit A to ca 45 % in unit B. This unit indicates the thickest glacial varves in the whole core. Glacial varves become thinner and finer downward through unit B. Summer layers are greatly thicker and coarser than winter layers. Since the most sediment is deposited during the summer when lots of meltwater is produced, coarser sediment such as sand and silt settle across the floor of the lake. But during the winter when the melting stops, finer particles such as clay settle in the lake and produce a distinct winter layer. Unit B coincides with Yoldia sea fresh water stage at the beginning of the Holocene warming, and the higher deposition rate with coarser sediment due to warmer climate is characteristic in this unit. The sediment core location was close to the receding ice sheet (Figure 25) and the receiving sediment from meltwater was huge.

A reverse trend starts at the beginning of unit C. The sediment becomes gradually coarser downward through the subunit C1 (silt ca. 70% - 40% and clay ca. 35% - 65%) and becomes almost stable from subunit C2 to end of the core (Figure 17). Glacial varves become thinner and lighter gradually downward through the rest of core. Subunit C3 and C2 occurred before BIL final drainage, and coarser sediment is a characteristic feature for these pre-drainage subunits

(silt ca. 40% - 70% and clay ca. 30% - 50%). At the bottom of subunit C1 the BIL final drainage is interpreted to have occurred at 309.8 cm depth. Post drainage sediment become finer and varve thickness increase gradually upward in subunit C1. Summer and winter layers have almost equal thickness in each varve through subunits C2 and C3 due to colder climate conditions and less sediment deposition. Sharper sand peaks in the sand percent's graph indicate that the sediment core site was located near the ice- margin before the drainage. But the sand peaks became milder during the post drainage varves. The biggest difference between C3 and C2 is the distance between summer and winter layers in silt and clay graphs (Figure 17), otherwise they have almost equal magnetic susceptibility and bulk density values. The summer and winter graphs (silt and clay) in C2 are closer to each other and the distance between these graphs become larger in C3. The variance between summer and winter layer samples were measured. The mean variance for subunit C2 is 15 % while the mean variance for subunit C3 is 30 %. The sand graph in figure 17 displays less variation through each varve compared to the silt and clay graph but there is still a big difference between the sharp sand points in each unit. The sharp sand points in C1 reach up to 3% while in C2 and C3 attain to 12%-15%, showing that the pre-drainage varves have a higher content of sand particles. The same pattern was also observed by Johnsson et al. (2013) in a varve sequence near Götene, Sweden; post-drainage varves were finer compared to pre-drainage. Their analysis consists of five post-drainage varves and five pre-drainage varves. They have taken several samples in each varve (between 4-7 samples). Silt percent in the pre-drainage varves were between 20 % - 50 % and clay 50 % - 80 %; post-drainage silt were 10 % - 30 % and clay were 70 % - 95 % in their results. The difference between pre-drainage and post-drainage sediments, including the difference between silt and clay values in summer and winter layers, is greater in their results because their sediment core position is closer to the drainage location at Mt Billingen than the current Askö sediment core (Asko2017HT-02-GC-1). The color change between pre-drainage and post-drainage are more obvious in Götene than Askö but in both studies coincide exactly with the grain size change. In the previous study by Brunnberg (1995) the color change appears at different times in different records which could be depending on bedrock source, erosion or different sediment source locations. The domination of very fine sand and silt particles display a relatively low energy condition in the whole core except unit A which indicates less sorted sand and silt particles. Coarser sediment amounts are higher in this unit than the rest of the core which represent a higher energy accumulation environment. Unit A is a very poorly sorted sediment which is interpreted to have deposited quickly or close to its source (glacial clay). But unit B and C shows finer sediments and slightly better sorting (poorly sorted) display a lower energy flow condition or a longer distance to its origin (Figure 20). The domination of finer silt and clay particles could be explained by longer distance to the source compared to (granules, pebbles and cobbles sediment), and that the sediment was sorted during its longer transport (units B and C).

4.4.Organic C & N and color changes

Changes in silt and clay percent and the organic carbon and nitrogen content coincide with the altered glacial varve color. Darker varves contains more organic carbon and nitrogen and at the same time include more fine particles. Pre-drainage winter layers which have a brownish red color and summer layers with lighter brownish color indicate less organic content and finer sediment particles due to BIL cold freshwater conditions (unit C). Post drainage winter layers have a greyish brown color and darker brownish summer layers which indicate more organic carbon and coarser sediment because of Yoldia Sea condition (unit B). Johnsson et al. (2013)

show the same results. Mineral variations may give different color in glacial varves, for example varve thickness is almost equal in unit C1 but they have differences color which can depend on both organic content percent and also type of sedimentary deposition.

Unit A is post glacial Gytja-clay which contains of high amounts of biogenic material. This unit contains probably the most nitrogen and organic carbon compare to pre- and post- glacial varves. Glacial clays that were located on shallow bottoms became eroded and were deposited as postglacial clay. This coring site is located in such an area. These younger postglacial clays contain organic material from the plants and algae that have lived in sea and lakes. Such sediments are still deposited today in the Baltic Sea.

Both pre-drainage and post drainage winter samples show higher values of organic carbon content. This can be explained by the fact that diatoms and phytoplankton bloom during the spring and grow rapidly during summer. Less daylight during the autumn change the conditions and diatoms and phytoplankton start to sink down. Therefore, winter layers indicate more organic carbon content than summer layers (Miller et al. 2011, Grosselin et al. 1997, Krembs et al. 2002). There is also a larger difference in organic carbon content between summer and winter layers after the drainage. The ice formation starts at the beginning of winter, rapidly rising salinity and making less advection, which presents higher values of organic carbon content in the graph (Figure 20).

The nitrogen content percent shows the same pattern as the organic carbon percent (Figure 21) in both pre-drainage and post drainage varves (Figure 22). The post-drainage varves have a higher total nitrogen content (ca. 0.03-0.06) than the pre-drainage varves (ca. 0.005- 0.03). As well as both pre- and post- drainage winter samples show higher values of nitrogen content because of early melt season. Based on the varve chronology for the core, unit C were predominantly deposited in the late Baltic Ice Lake stage during the Younger Dryas. Post-drainage varves contained more organic matter compared to pre-drainage in Johnson et al. (2013) which correspond to the results of this study.

5. Conclusions

The Paleo environmental record interpreted from varve thickness measurements, grain size variations and total C & N content in core Asko2017HT-02-GC-1 is presented below:

The core indicated 299 glacial varves. By connection between the varve thickness diagram and the four nearest varve diagrams from Brunnberg (1995), the estimated age for this core spans from 11488 to 11787 cal yr BP.

Three distinct lithological units are observed in this core. Unit C was deposited predominantly during the end of the Baltic Ice Lake stage (fresh water) during the Younger Dryas by a varve thickness about 9 mm (pre-drainage). Unit C is divided into 3 subunits. The BIL final drainage is recorded at the border between unit C1 and C2 (1594 cal yr BP) which is 26 years younger than the most recent published value (Stroven et al., 2015). Unit B display a rapidly ice recession after the BIL final drainage. A higher deposition rate was recorded at the beginning of Holocene warming climate and formed the thickest glacial varves in this unit (between 4-6 cm thickness)

during the Yoldia Sea stage fresh water phase. Unit A represent post glacial clay at the top of the core.

Post-drainage varves in core Asko2017HT-02-GC-1 are finer, more dark brown in color and contains more carbon and nitrogen compared to pre-drainage varves, which correspond to results by Johnsson et al. (2013). There is a relationship between grain size variation and carbon and nitrogen values in both studies. Post-drainage glacial varves demonstrate a higher carbon and nitrogen values compared to pre-drainage sediments (Figure 16 and 17). Winter layers also indicate higher carbon and nitrogen values compared to summer layers because diatoms and phytoplankton bloom in the spring/summer and sink in the autumn/winter.

Summer layers have coarser sediment through the whole core in the 344 measured samples. But some few points show a reverse trend which could be caused by some intra-seasonal storm events or that some winters became warmer. Summer layers are thicker than winter layers in unit B but become thinner downward in this unit. Summer and winter layers have almost equal thickness in unit C. Statistical analysis by GRADISTAT Version 8.0 shows the same trends and unit division as the particle size distribution. Units B and C have generally finer sediments (finer silt in summer to clay in winter) and display better sorting than unit A (poorly sorted compared to very poorly sorted in unit A) and also shows milder kurtosis graph (from mesokurtic on summer layers and platykurtic on winter layers to leptokurtic-mesokurtic in unit A).

Since the core location lies in a higher area compared to surrounding area it is exposed to an ongoing erosion of the seafloor on the top of this core in unit A. The whole core except unit A consists mostly of clay and very fine silt which has low permeability. Sorting analysis shows poorly sorted sediments through the whole core except unit A which is very poorly sorted. Since most of units B and C indicate very fine silt and almost equal amounts of clay and silt particles, it formed a low permeability sediment. The connection between pores is low and clay tends to hold water, and as a result water moves slower downward through unit B and C compared to unit A which has a higher permeability (medium silt).

It is reasonable that the sand layer on the top of unit B (that represent a hiatus) is a more permeable layer which could have hosted groundwater flow. It shows leptokurtic distribution (chiefly sand particles) and is very coarse skewed and a better sorted compared to units B and C.

More research is needed to give a better pattern of groundwater flow in the study area. Future work could be studies of the second core to find more possible evidence of groundwater seepage. However, an accurate estimation of groundwater resource needs more investigation both on geophysical data and sediments sampling in the Askö region.

Acknowledgements

I gratefully acknowledge my supervisor Dr Richard Gyllencreutz who helped me throughout this project and without him I could not manage this thesis. Heike Sigemund for helping me with the C/N analysis and Carina Johansson for helping me with the sample preparation with Malvern instrument. at Stockholm University.

I would like to thank Professor Martin Jakobsson, Dr Matt O'Regan and again Dr Richard Gyllencreutz for coring and retrieving of this unique sample during the marine geological mapping with geophysical methods and sediment sampling course. Finally, I would also like to thank my amazing family for supporting and encouragement during this project.

References

- Adrielson, L. (1984). Weichselian lithostratigraphy and glacial environments in the Ven-Glumslövårea, southern Sweden. Lundqua, Thesis 16. Department of Geology, Lund University, 120.
- Andrews, S., Nover, D., Schladow, G. (2010). Using laser diffraction data to obtain accurate particle size distributions: the role of particle composition. *Limnology and Oceanography Methods*, 507-526. doi: 10.4319/lom.2010.8.507.
- Andrén, E., Andrén, T., Kunzendorf, H. (2000a). Holocene history of the Baltic Sea as a background for assessing records of human impact in the sediments of the Gotland Basin. *The Holocene* 10, 687-702. doi: 10.1191/09596830094944.
- Andrén, T., Andrén E., Berglund, B.E. (2007b). New insights on the Yoldia Sea low stand in the Blekinge archipelago, southern Baltic Sea. *GFF* 129. 273-281. doi: 10.1080/11035890701294277.
- Andrén, T., Björck, S., Andrén, E., Conley, D., Zillén, L. & Anjar, J. (2011). The development of the Baltic Seabasin during the last 130 ka. In Harff, J., Björck, S. & Hooth, P. (eds.): *The Baltic Sea Basin*, 75–98. Springer-Verlag, Berlin and Heidelberg.
- Andrén, T., Björck, J., Johnsen, S. (1999). Correlation of Swedish glacial varves with the Greenland (GRIP) oxygen isotope record. *Journal of Quaternary Science*, Vol. 14, 361-371. doi: 10.1002/(sici)1099-1417(199907)14:4<361::aid-jqs446>3.0.co;2-r.
- Andrén, T. (2003a). Baltiska Issjön – eller hur det började (The Baltic Ice Lake – or how it began), *Havsutsikt* 1, 4-5. (in Swedish).
- Andrén, T., Lindeberg, G. & Andrén, E. (2002). Evidence of the final drainage of the Baltic Ice Lake and the brackish phase of the Yoldia Sea in glacial varved from the Baltic Sea. *Boreas* 31, 226–238. doi:10.1111/j.1502-3885.2002.tb01069.x.
- Beard, D. C., Weyl, P. K. (1973). Influence of Texture on Porosity and Permeability of Unconsolidated Sand, *AAPG Bulletin* 57, 349-369. doi: 10.1306/819a4272-16c5-11d7-8645000102c1865d.
- Berglund, B.E., Sandgren, P., Barnekow, L., Hannon, G., Jiang, H., Skog, G., Yu, S. (2005). Early Holocene history of the Baltic Sea, as reflected in coastal sediments in Blekinge, southeastern Sweden. *Quaternary International* 130, 111-139. doi: 10.1016/j.quaint.2004.04.036.

- Bergström, R. (1968). Stratigrafi och is recession i södra Västerbotten. Sveriges Geologiska Undersökning, C 634, 1-76.
- Bianchi, T.S., Westman, P., Rolff, C., Engelhaupt, E., André, T., Elmgren, R. (2000). Cyanobacterial blooms in the Baltic Sea: natural or human-induced? *Limnology and Oceanography* 45, 716-726. doi: 10.4319/lo.2000.45.3.0716.
- Björck, S. (2008). The late Quaternary development of the Baltic Sea basin. In *Assessment of climate change for the Baltic Sea Basin* Edited by: The BACC Author Team, 398–407. Springer-Verlag, Berlin and Heidelberg.
- Björck, S., Rasmussen, T., Kromer, B., Johnsen, S., Hammer, C., Bennike, O., Hammarlund, D., Lemdahl, G., Wohlfarth, B., Possnert, G., & Spurk, M. (1996). Synchronized terrestrial atmospheric deglacial records around the North Atlantic, *Science* 274(5290), 1155-1160. doi:10.1126/science.274.5290.1155.
- Björck, S. (1995). A review of the history of the Baltic Sea, 13.0-8.0 ka BP. *Quaternary International* 27, 19-40. doi:10.1016/1040-6182(94)00057-C.
- Björck, S., Rundgren, M., Ingolfsson, O., Funder, S. (1997). The Preboreal Oscillation around the Nordic Seas: terrestrial and lacustrine responses. *Journal of Quaternary Science* 12, 455-466. doi: 10.1002/(sici)1099-1417(199711/12)12:6<455::aid-jqs316>3.0.co;2-s.
- Blott, S. J., Pye, K. (2001). GRADISTAT: a grain size distribution and statistics package for the analysis of unconsolidated sediments. *Earth Surface Process and Landforms* 26, 1237-1248. doi: 10.1002/esp.261.
- Borgendahl, J., Westman, P. (2006). Cyanobacteria as a trigger for increased primary productivity during sapropel formation in the Baltic Sea – a study of the Ancyclus/Litorina transition. *Journal of Paleolimnology* 38, 1-12. doi: 10.1007/s10933-006-9055-0.
- Brunnberg, L. (1995). Clay-varve chronology and deglaciation during the Younger Dryas and Preboreal in the easternmost part of the Middle Swedish Ice Marginal Zone. PhD thesis, Quaternaria, Stockholm University, Stockholm, 1-94.
- Cato, I. (1987). On the definitive connection of the Swedish Time Scale with the present. *Geological Survey of Sweden. Ca* 68, 1-55.
- De Geer, G. (1884). Om den skandinaviska landisens andra utbredning, *Geologiska Föreningen i Stockholm Förhandlingar* 7:7, 436-466. doi: 10.1080/11035898409443544
- De Geer, G. (1940). *Geochronologia Suecica Principles*. Kungliga Svenska Vetenskapsakademiens handlingar Ser III 18 (6), 367.
- Folk RL, Ward WC. (1957). Brazos River bar: a study in the significance of grain size parameters. *Journal of Sedimentary Petrology* 27, 3-26. doi: 10.1306/74d70646-2b21-11d7-8648000102c1865d.
- Fonselius, S. (1996). The upwelling of nutrients in the central Skagerrak. *Deep Sea Research Part II: Topical Studies in Oceanography* 43, 57-71. doi: 10.1016/0967-0645(95)00083-6.
- Galacgac, A., Ooi, P. (2018). Use of a Laser Diffractometer to Obtain the Particle Size Distribution of Fine-Grained Soils, *Transportation Research Record. The Journal of the Transportation Research Board, Hawaii, SAGE Publications*. doi: 10.1177/0361198118755712.
- Gosselin, M., Levasseur, M., Wheeler, P. A., Horner, R. A., and Booth, B. C. (1997). New measurements of phytoplankton and ice algal production in the Arctic Ocean. *Deep Sea Research Part II: Topical Studies in Oceanography* 44, 1623-1644, doi: 10.1016/S0967-0645(97)00054-4.
- Granberg, T. (2012). Grain size analysis- a comparison between laser and sedigraph analytical techniques, Bachelor thesis, department of geological sciences, Stockholm University, Stockholm.

- Gustafsson, B.G., Westman, P. (2002). On the causes for salinity variations in the Baltic Sea for the last 8500 years. *Paleoceanography* 17,1-14. doi: 10.1029/2000pa000572.
- Houmark-Nielsen, M., Kjær, K.H. (2003). Southwest Scandinavia, 40–15 ka BP: palaeogeography and environmental change. *Journal of Quaternary Science* 18, 769-786. doi: 10.1002/jqs.802.
- Jakobsson, M., Björck, S., Alm, G., Andrén, T., Lindeberg, G., Svensson, N.O. (2007). Reconstructing the Younger Dryas ice dammed lake in the Baltic Basin: Bathymetry, area and volume. *Global and Planetary Change* 57, 355-370. doi: 10.1016/j.gloplacha.2007.01.006.
- Jakobsson, M., O'Regan, M., Gyllencreutz, R., Flodén, T. (2016). Seafloor terraces and semi-circular depressions related to fluid discharge in Stockholm Archipelago, Baltic Sea. *Geological Society, London, Memoirs* 46, 305-306. doi: 10.1144/m46.162.
- Johnson, M.D., Addis, K.L., Ferber, L.R., Hemstad, C., Meyer, G.N. & Komai, L.T., (1999). Glacial Lake Lind, Wisconsin and Minnesota, USA. *Geological Society of America Bulletin* 111, 1371-1386. doi: 10.1130/0016-7606(1999)111<1371:gllwam>2.3.co;2.
- Johnson, M.D., Kylander, M.E., Casserstedt, L., Wiborgh, H. & Björck, S. (2013). Varved glaciomarine clay in central Sweden before and after the Baltic Ice Lake drainage: a further clue to the drainage events at Mt Billingen. *GFF* 135, 293–307. doi:10.1080/11035897.2013.
- Krembs, C., Eicken, H., Junge, K., and Deming, J. W. (2002). High concentrations of exopolymeric substances in Arctic winter sea ice: implications for the polar ocean carbon cycle and cryoprotection of diatoms. *Deep Sea Research Part I: Oceanographic Research Papers* 49, 2163-2181. doi: 10.1016/s0967-0637(02)00122-x.
- Kristiansson, J. (1986). The ice recession in the south-eastern part of Sweden. A varve chronological time scale for the latest part of the Late Weichselian. University of Stockholm, Department of Quaternary Research, Report 16, 1-132.
- Krumbein, W.C., Pettijohn, F.J. (1938). *Manual of Sedimentary Petrography*. Appleton-Century Crofts, Inc., New York.
- Kunzendorf, H., Voss, M., Brenner, W., Andrén, T., Vallius, H. (2001). Molybdenum in sediments of the central Baltic Sea as an indicator for algal blooms. *Baltica* 14, 123-130. doi: 10.1639/0044-7447(2001)030[0184:ehabas]2.0.co;2.
- Lambeck, K. (2001). Sea level change through the Last Glacial cycle. *Science* 292, 679-686. doi: 10.1126/science.1059549.
- Lebrun, D., Belaid, S., Ozkul, C., Ren, K., Grehan, G. (1996). Enhancement of wire diameter measurements: comparison between Fraunhofer diffraction and Lorenz-Mie theory. *Optical Engineering* 35(4), 946. doi: 10.1117/1.600703.
- Lockhart, Edward. (2015). *The Geotechnical Investigation of Glacigenic Sediments in the Celtic Sea*. doi: 10.13140/RG.2.1.2295.9442/1.
- Lowe, J., Walker, M. (2014). *Reconstructing Quaternary Environments*, London, Routledge.
- Malvern Instruments Ltd, 2011, *Mastersizer 3000 User Manual, Brochure*, Elsevier BV, Enigma Business Park, United Kingdom.
- Miller, L. A., Papakyriakou, T. N., Collins, R. E., Deming, J. W., Ehn, J. K., Macdonald, R. W., Mucci, A., Owens, O., Raudsepp, M., and Sutherland, N. (2011). Carbon dynamics in sea ice: A winter flux time series. *Journal of Geophysical Research*, 116, C02028. doi:10.1029/2009JC006058.

- Muschitiello, F., Smittenberg, R., Wohlfarth, B., Pausata, F., Salih, A., Watson, J., Whitehouse, N., Brooks, S. & Karlatou Charalampopoulou, A. (2015). Fennoscandian freshwater control on Greenland hydroclimate shifts at the onset of the Younger Dryas. *Nature Communications*, 6:8939. doi: 10.1038/ncomms9939.
- Piotrowski, J.A. (1997). Subglacial hydrology in north-western Germany during the last glaciation: groundwater flow, tunnel valleys and hydrological cycles, *Quaternary Science Reviews*. *Quaternary Science Reviews* 16, 169-185. doi:10.1016/s0277-3791(96)00046-7.
- Ridge, J.C., & Larsen, F.D. (1990). Re-evaluation of Antevs' New England varve chronology and new radiocarbon dates of sediments from glacial Lake Hitchcock. *Geological Society of America Bulletin* 102, 889-899. doi: 10.1130/0016-7606(1990)102<0889:reokane>2.3.co;2.
- Saarnisto, M., Saarinen, T. (2001). Deglaciation chronology of the Scandinavian ice sheet from the Lake Onega basin to the Salpausselkä end moraines. *Global Planetary Change* 31, 387-405. doi: 10.1016/s0921-8181(01)00131-x.
- Seifert, Torsten & Kayser, B. (1995). A High Resolution Spherical Grid Topography of the Baltic Sea. *Meereswissenschaftliche Berichte*, 72-88.
- Schoning, K., Wastegård, S. (1999). Ostracod assemblages in late Quaternary varved glaciomarine clay of the Baltic Sea Yoldia stage in eastern middle Sweden. *Marine Micropaleontology* 37, 313-325. doi: 10.1016/s0377-8398(99)00027-4.
- Sohlenius, G., Emeis, K.C., Andrén, E., Andrén, T., Kohly, A. (2001). Development of anoxia during the, fresh-brackish water transition in the Baltic Sea. *Marine Geology* 177, 221-242. doi: 10.1016/s0025-3227(01)00174-8.
- Sohlenius, G., Westman, P. (2008). Salinity and redox alternations in the northwestern Baltic proper during the late Holocene. *Boreas* 27, 101-114. doi: 10.1111/j.1502-3885.1998.tb00871.x.
- St-Onge, G., Mulder, T., Francus, P., Long, B. (2007). Continuous Physical Properties of Cored Marine Sediments. Proxies in late cenozoic paleoceanography, Elsevier, Amsterdam, 63-92.
- Stevens, R. (2008). Glaciomarine varves in late-Pleistocene clays near Göteborg, southwestern Sweden. *Boreas* 14, 127-132. doi: 10.1111/j.1502-3885.1985.tb00904.x.
- Stroeven, A.P., Heyman, J., Fabel, D., Björck, S., Caffee, M.W., Fredin, O. & Harbor, J.M. (2015). A new Scandinavian reference ¹⁰Be production rate. *Quaternary Geochronology* 29, 104-115. doi: 10.1016/j.quageo.2015.06.011.
- Strömberg, B. (1992). The final stage of the Baltic Ice Lake. In: *Late Quaternary stratigraphy glacial morphology and environmental changes* (eds. A.-M. Robertson, B. Ringberg, U. Miller, L. Brunnberg). *Sveriges Geologiska Undersökning Ca.* 81, 347-354.
- Tavenas, F., Jean, p., Leblond, P., Leroueil, S. (1984). The permeability of natural soft clays. Part II: Permeability characteristics: Reply. *Canadian Geotechnical Journal* 21, 645-732. doi: 10.1139/t84-082.
- Voipio, A. (ed) (1981). *The Baltic Sea*. Amsterdam. Elsevier oceanography series 30.
- Voss, M., Kowalewska, G., Brenner, W. (2001). Microfossil and biochemical indicators of environmental changes in the Gotland Deep during the last 10,000 years. *Baltica* 14, 131-140.
- Weckström, K., Saunders, K., Gell, P., and Skilbeck, C. (2017). Applications of paleo environmental techniques in estuarine studies, Chapter 24, 615-700. doi:10.1007/978-94-024-0990-1.
- Wentworth, C.K. (1922). A scale of grade and class terms for clastic sediments. *The Journal of Geology* 30, 377-392. doi: 10.1086/622910.

Wessels, M. (1998). Natural environmental changes indicated by Late Glacial and Holocene sediments from Lake Constance, Germany. *Palaeogeography, Palaeoclimatology, Palaeoecology* 140, 421-432. doi: 10.1016/s0031-0182(98)00026-1.

Westman, P., Sohlenius, G. (1999). Diatom stratigraphy in five off-shore sediment cores from the northwestern Baltic proper implying large-scale circulation changes during the last 8500 years, *Journal of Paleolimnology* 22, 53-69.

Winsor P., Rodhe J., Omstedt A. (2001). Baltic Sea ocean climate: an analysis of 100 yr of hydrographic data with focus on the freshwater budget. *Climate Research* 18, 5-15. doi: 10.3354/cr018005.

Winterhalter, B. (1992). Late-Quaternary stratigraphy of Baltic Sea basins - a review. *Bulletin of the Geological Society of Finland* 64, 189-194. doi: 10.17741/bgsf/64.2.007.

Winterhalter, B., Flodén, T., Ignatius, H., Axberg, H., Niemistö, H. (1981). *The Baltic Sea*, Elsevier, 1-121. Voipio (Ed.), Amsterdam.

Wohlfarth, B., Björck, S., Possnert, G. & Holmquist, B. (1998). An 800-year long, radiocarbon-dated varve chronology from south-eastern Sweden. *Boreas* 27, 243-257.

Zillén, L., Conley, D.J., Andrén, T., Andrén, E., Björck, S. (2008). Past occurrences of hypoxia in the Baltic Sea and the role of climate variability, environmental change and human impact. *Earth Science Reviews* 91, 77-92. doi: 10.1016/j.earscirev.2008.10.001.

Zillén, L., Conley, D.J. (2010). Hypoxia and cyanobacteria blooms - are they really natural features of the late Holocene history of the Baltic Sea? *Biogeosciences* 7, 2567-2580. doi: 10.5194/bg-7-2567-2010.

Appendix

Appendix 1: Varve chronology in three different time scales.

Varves from top to bottom	Start	Unclear Boundaries	Layer thickness	Stroeven 2015 (cal yr BP)	De Geer (STS)	Cato 1987 (clay yr BP)
1	31.5		5.6	11488	1398	10638
2	37.1		4.3	11489	1399	10639
3	41.4		3.6	11490	1400	10640
4	45		4	11491	1401	10641
5	49	?	5	11492	1402	10642
6	54		4.3	11493	1403	10643
7	58.3		3.7	11494	1404	10644
8	62		5.5	11495	1405	10645
9	67.5		4.8	11496	1406	10646
10	72.3		2.7	11497	1407	10647
11	75		3.1	11498	1408	10648
12	78.1		1.2	11499	1409	10649
13	79.3		5.5	11500	1410	10650
14	84.8		1.3	11501	1411	10651
15	86.1		1.4	11502	1412	10652
16	87.5		2.6	11503	1413	10653
17	90.1		3	11504	1414	10654
18	93.1		4.2	11505	1415	10655
19	97.3		3.3	11506	1416	10656
20	100.6		4.6	11507	1417	10657
21	105.2		5.2	11508	1418	10658
22	110.4	?	6	11509	1419	10659
23	116.4		3.3	11510	1420	10660
24	119.7		3.8	11511	1421	10661
25	123.5		4.1	11512	1422	10662
26	127.6		1.4	11513	1423	10663

27	129		3.8	11514	1424	10664
28	132.8		3.3	11515	1425	10665
29	136.1	?	4.1	11516	1426	10666
30	140.2	?	3.6	11517	1427	10667
31	143.8		3.9	11518	1428	10668
32	147.7		3.2	11519	1429	10669
33	150.9		3.2	11520	1430	10670
34	154.1		5	11521	1431	10671
35	159.1		5.8	11522	1432	10672
36	164.9		3.6	11523	1433	10673
37	168.5		6.9	11524	1434	10674
38	175.4		8.1	11525	1435	10675
39	183.5		8.3	11526	1436	10676
40	191.8		3.3	11527	1437	10677
41	195.1		2.9	11528	1438	10678
42	198		4	11529	1439	10679
43	202		3.5	11530	1440	10680
44	205.5		3.5	11531	1441	10681
45	209		3.7	11532	1442	10682
46	212.7		1.1	11533	1443	10683
47	213.8		2.6	11534	1444	10684
48	216.4		1.6	11535	1445	10685
49	218		1.5	11536	1446	10686
50	219.5		1	11537	1447	10687
51	220.5		2.1	11538	1448	10688
52	222.6		1.9	11539	1449	10689
53	224.5		3.4	11540	1450	10690
54	227.9		1.5	11541	1451	10691
55	229.4		2.3	11542	1452	10692
56	231.7		2.1	11543	1453	10693
57	233.8		1.4	11544	1454	10694
58	235.2		3.3	11545	1455	10695
59	238.5		2.2	11546	1456	10696
60	240.7		1.8	11547	1457	10697
61	242.5		1.5	11548	1458	10698
62	244		2.2	11549	1459	10699
63	246.2		2.5	11550	1460	10700
64	248.7		2.7	11551	1461	10701
65	251.4		1	11552	1462	10702
66	252.4		2.7	11553	1463	10703
67	255.1		0.9	11554	1464	10704
68	256		1.7	11555	1465	10705
69	257.7		1.4	11556	1466	10706
70	259.1		0.9	11557	1467	10707
71	260		1.9	11558	1468	10708
72	261.9		1.5	11559	1469	10709
73	263.4		1	11560	1470	10710
74	264.4	?	1.9	11561	1471	10711
75	266.3		2.2	11562	1472	10712
76	268.5		1	11563	1473	10713
77	269.5	?	1	11564	1474	10714
78	270.5		1.5	11565	1475	10715
79	272		1.1	11566	1476	10716
80	273.1		1.6	11567	1477	10717
81	274.7		1.7	11568	1478	10718
82	276.4		1.4	11569	1479	10719
83	277.8		0.6	11570	1480	10720
84	278.4		1.4	11571	1481	10721
85	279.8		1.5	11572	1482	10722
86	281.3		2.3	11573	1483	10723
87	283.6		1.2	11574	1484	10724
88	284.8		2.5	11575	1485	10725
89	287.3		1.7	11576	1486	10726
90	289		1.1	11577	1487	10727
91	290.1		1.1	11578	1488	10728
92	291.2		1.1	11579	1489	10729

93	292.3		1.1	11580	1490	10730
94	293.4		1.4	11581	1491	10731
95	294.8		1.6	11582	1492	10732
96	296.4		1.2	11583	1493	10733
97	297.6	?	1.2	11584	1494	10734
98	298.8	?	1	11585	1495	10735
99	299.8		1.1	11586	1496	10736
100	300.9		1	11587	1497	10737
101	301.9		1.1	11588	1498	10738
102	303		1.2	11589	1499	10739
103	304.2		1.8	11590	1500	10740
104	306		1.6	11591	1501	10741
105	307.6		0.9	11592	1502	10742
106	308.5		1.3	11593	1503	10743
107	309.8		1.2	11594	1504	10744
108	311		0.8	11595	1505	10745
109	311.8	?	1.2	11596	1506	10746
110	313		1.1	11597	1507	10747
111	314.1		1.2	11598	1508	10748
112	315.3		1.7	11599	1509	10749
113	317		0.7	11600	1510	10750
114	317.7		1.1	11601	1511	10751
115	318.8		0.3	11602	1512	10752
116	319.1		0.4	11603	1513	10753
117	319.5		0.6	11604	1514	10754
118	320.1		0.9	11605	1515	10755
119	321		1	11606	1516	10756
120	322		1	11607	1517	10757
121	323		1.1	11608	1518	10758
122	324.1		0.9	11609	1519	10759
123	325		1.6	11610	1520	10760
124	326.6		0.7	11611	1521	10761
125	327.3		1.4	11612	1522	10762
126	328.7		1.5	11613	1523	10763
127	330.2		0.7	11614	1524	10764
128	330.9		0.7	11615	1525	10765
129	331.6		1.1	11616	1526	10766
130	332.7		1.7	11617	1527	10767
131	334.4		0.8	11618	1528	10768
132	335.2		0.8	11619	1529	10769
133	336		0.9	11620	1530	10770
134	336.9		1	11621	1531	10771
135	337.9		1	11622	1532	10772
136	338.9		0.5	11623	1533	10773
137	339.4		1.8	11624	1534	10774
138	341.2		0.8	11625	1535	10775
139	342		1.3	11626	1536	10776
140	343.3		0.9	11627	1537	10777
141	344.2		1.4	11628	1538	10778
142	345.6		0.6	11629	1539	10779
143	346.2		1.1	11630	1540	10780
144	347.3		0.7	11631	1541	10781
145	348		0.7	11632	1542	10782
146	348.7		0.6	11633	1543	10783
147	349.3		0.7	11634	1544	10784
148	350		1	11635	1545	10785
149	351		1	11636	1546	10786
150	352		0.8	11637	1547	10787
151	352.8		1.2	11638	1548	10788
152	354		0.9	11639	1549	10789
153	354.9		0.8	11640	1550	10790
154	355.7		1.3	11641	1551	10791
155	357		1	11642	1552	10792
156	358		1	11643	1553	10793
157	359		1.1	11644	1554	10794
158	360.1		0.9	11645	1555	10795

159	361		0.5	11646	1556	10796
160	361.5		0.5	11647	1557	10797
161	362		1	11648	1558	10798
162	363		1	11649	1559	10799
163	364		1.5	11650	1560	10800
164	365.5		0.6	11651	1561	10801
165	366.1		1.1	11652	1562	10802
166	367.2		0.8	11653	1563	10803
167	368		1	11654	1564	10804
168	369		0.5	11655	1565	10805
169	369.5		0.5	11656	1566	10806
170	370		0.6	11657	1567	10807
171	370.6		1.4	11658	1568	10808
172	372		1	11659	1569	10809
173	373		1	11660	1570	10810
174	374		1	11661	1571	10811
175	375		1	11662	1572	10812
176	376		1.1	11663	1573	10813
177	377.1		1	11664	1574	10814
178	378.1		1.6	11665	1575	10815
179	379.7		1.3	11666	1576	10816
180	381		0.9	11667	1577	10817
181	381.9		0.9	11668	1578	10818
182	382.8		1.5	11669	1579	10819
183	384.3		1.2	11670	1580	10820
184	385.5		1.4	11671	1581	10821
185	386.9	?	1.9	11672	1582	10822
186	388.8		0.7	11673	1583	10823
187	389.5		1.4	11674	1584	10824
188	390.9		0.5	11675	1585	10825
189	391.4		0.5	11676	1586	10826
190	391.9		0.5	11677	1587	10827
191	392.4		1.6	11678	1588	10828
192	394		0.9	11679	1589	10829
193	394.9		0.9	11680	1590	10830
194	395.8		0.9	11681	1591	10831
195	396.7		1.1	11682	1592	10832
196	397.8		1.2	11683	1593	10833
197	399		0.9	11684	1594	10834
198	399.9		0.9	11685	1595	10835
199	400.8		0.3	11686	1596	10836
200	401.1		1.4	11687	1597	10837
201	402.5		1	11688	1598	10838
202	403.5		2.1	11689	1599	10839
203	405.6		1.1	11690	1600	10840
204	406.7		1	11691	1601	10841
205	407.7		0.9	11692	1602	10842
206	408.6		0.4	11693	1603	10843
207	409		0.4	11694	1604	10844
208	409.4		0.6	11695	1605	10845
209	410		0.5	11696	1606	10846
210	410.5		0.6	11697	1607	10847
211	411.1		0.9	11698	1608	10848
212	412		1	11699	1609	10849
213	413		1.5	11700	1610	10850
214	414.5		0.5	11701	1611	10851
215	415		1	11702	1612	10852
216	416		1	11703	1613	10853
217	417		1	11704	1614	10854
218	418		0.7	11705	1615	10855
219	418.7		0.7	11706	1616	10856
220	419.4		1.4	11707	1617	10857
221	420.8	?	1.2	11708	1618	10858
222	422	?	1	11709	1619	10859
223	423		0.9	11710	1620	10860
224	423.9		1	11711	1621	10861

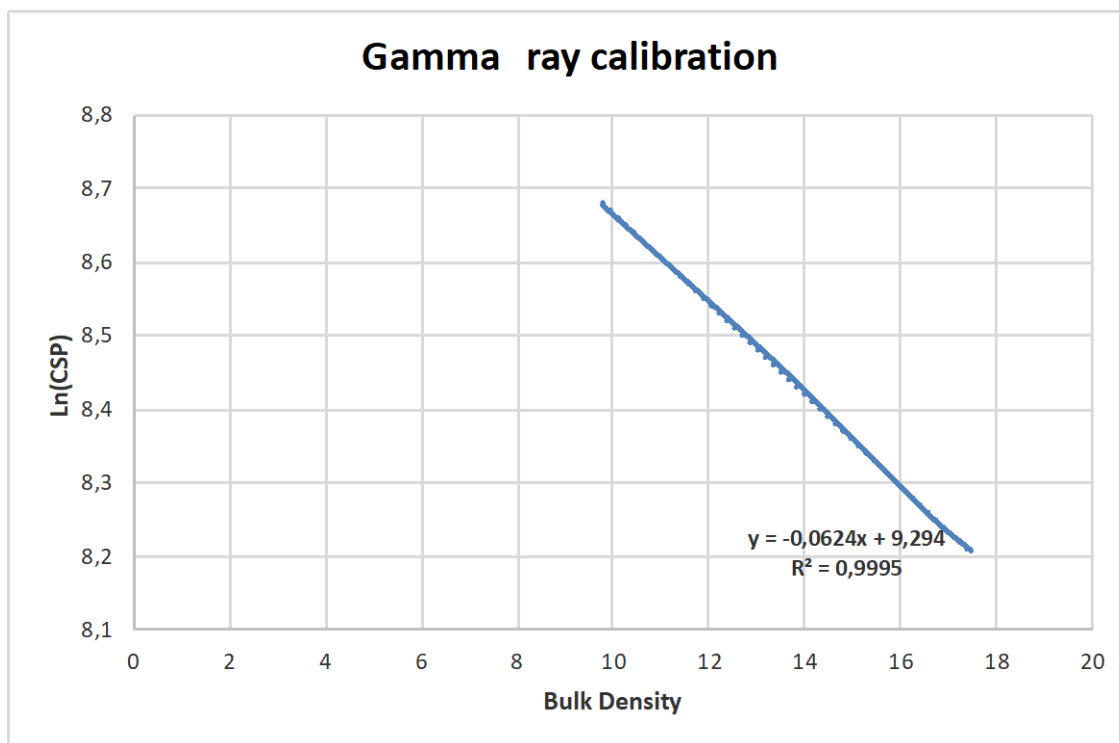
225	424.9		1.3	11712	1622	10862
226	426.2		0.9	11713	1623	10863
227	427.1		0.8	11714	1624	10864
228	427.9		0.6	11715	1625	10865
229	428.5		1	11716	1626	10866
230	429.5		1	11717	1627	10867
231	430.5	?	0.8	11718	1628	10868
232	431.3		0.9	11719	1629	10869
233	432.2		1	11720	1630	10870
234	433.2		0.8	11721	1631	10871
235	434		1	11722	1632	10872
236	435		1	11723	1633	10873
237	436		0.6	11724	1634	10874
238	436.6		0.6	11725	1635	10875
239	437.2		0.8	11726	1636	10876
240	438	?	1	11727	1637	10877
241	439		1.2	11728	1638	10878
242	440.2		1.1	11729	1639	10879
243	441.3	?	0.8	11730	1640	10880
244	442.1		0.7	11731	1641	10881
245	442.8	?	0.7	11732	1642	10882
246	443.5		0.7	11733	1643	10883
247	444.2		1.4	11734	1644	10884
248	445.6		1.4	11735	1645	10885
249	447		0.9	11736	1646	10886
250	447.9		0.7	11737	1647	10887
251	448.6		2	11738	1648	10888
252	450.6		0.6	11739	1649	10889
253	451.2		1.4	11740	1650	10890
254	452.6		0.9	11741	1651	10891
255	453.5		1.5	11742	1652	10892
256	455		1	11743	1653	10893
257	456		1	11744	1654	10894
258	457		1	11745	1655	10895
259	458		3	11746	1656	10896
260	461		2.8	11747	1657	10897
261	463.8		0.7	11748	1658	10898
262	464.5		0.5	11749	1659	10899
263	465		2	11750	1660	10900
264	467		2	11751	1661	10901
265	469		1.7	11752	1662	10902
266	470.7		1	11753	1663	10903
267	471.7		0.5	11754	1664	10904
268	472.2		1.3	11755	1665	10905
269	473.5		1	11756	1666	10906
270	474.5		0.6	11757	1667	10907
271	475.1		0.6	11758	1668	10908
272	475.7		0.6	11759	1669	10909
273	476.3		0.9	11760	1670	10910
274	477.2		0.8	11761	1671	10911
275	478		0.8	11762	1672	10912
276	478.8		0.9	11763	1673	10913
277	479.7		0.7	11764	1674	10914
278	480.4		0.9	11765	1675	10915
279	481.3		1	11766	1676	10916
280	482.3		1.8	11767	1677	10917
281	484.1		0.8	11768	1678	10918
282	484.9		0.9	11769	1679	10919
283	485.8		1.1	11770	1680	10920
284	486.9		0.8	11771	1681	10921
285	487.7		0.8	11772	1682	10922
286	488.5		0.7	11773	1683	10923
287	489.2		0.8	11774	1684	10924
288	490		1.6	11775	1685	10925
289	491.6		1.8	11776	1686	10926
290	493.4		0.6	11777	1687	10927

291	494		1.9	11778	1688	10928
292	495.9		1.9	11779	1689	10929
293	497.8		0.2	11780	1690	10930
294	498		0.4	11781	1691	10931
295	498.4		0.6	11782	1692	10932
296	499		0.7	11783	1693	10933
297	499.7		1.4	11784	1694	10934
298	501.1		1	11785	1695	10935
299	502.1		1	11786	1696	10936
300	503.1		1	11787	1697	10937

Appendix 2:

No	Position	ACID TREATED (porv:cm)	Vikt mg	NOT ACID TREATED (prov:cm)	Vikt mg	Labb nr	$\delta^{13}\text{C}_{\text{org}}$ vs PDB (‰)	% Corg	$\delta^{15}\text{N}$ vs air (‰)	% N
1	A5	S 34	20.468	S 34	20.546	5	-26.79	0.41	nd	0.037
2	B1	S 44	20.421	S 44	20.564	7	-27.12	0.26	nd	0.025
3	A4	S 302.5	20.354	S 302.5	20.53	4	-26.84	0.14	nd	0.015
4	C2	S 305.5	20.234	S 305.5	20.433	14	-27.03	0.11	nd	0.006
5	A1	S 308.2	20.438	S 308.2	20.693	1	-27.86	0.11	nd	0.006
6	B3	S 310.5	20.378	S 310.5	20.483	9	-26.86	0.14	nd	0.008
7	B6	S 314	20.584	S 314	20.247	12	-27.04	0.10	nd	0.007
1	A6	V 37.1	20.145	V 37.1	20.239	6	-27.54	0.40	nd	0.058
2	B2	V 48.5	20.446	V 48.5	20.48	8	-27.52	0.46	nd	0.059
3	A3	V 303	20.237	V 303	20.262	3	-27.74	0.37	nd	0.048
4	C1	V 306	20.577	V 306	20.546	13	-27.49	0.29	nd	0.038
5	A2	V 308.5	20.542	V 308.5	20.422	2	-27.74	0.25	nd	0.033
6	B4	V 311	20.239	V 311	20.385	10	-27.20	0.22	nd	0.029
7	B5	V 314.3	20.579	V 314.3	20.269	11	-27.42	0.19	nd	0.024

Appendix 3:



Gamma ray density = cps;

$$\ln(\text{cps}) = -0.0624 * (\text{Density} * \text{Sediment Thickness}) + 9.294;$$

Re-arrange equation: $\text{Density} = [\ln(\text{cps}) - 9.294] / (-0.0624 * \text{sediment thickness}).$

Bulk dens	CSP	Ln (CSP)
9.8	5882	8.679652119
13.23	4790	8.47428569
14.896	4303	8.367067733
16.562	3851	8.256088134
17.444	3665	8.206583614